



People's Democratic Republic of Algeria  
Ministry of Higher Education and Scientific Research  
Med Khider University of Biskra  
Faculty of Exact Sciences and Sciences of Nature and Life

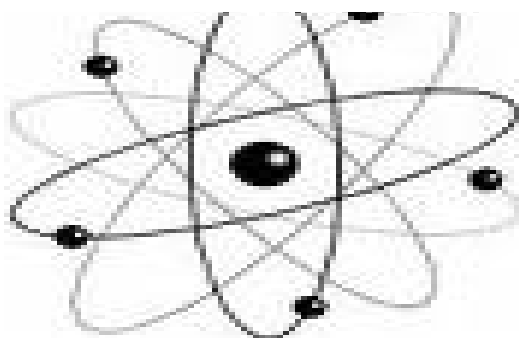


Matter Sciences Department

Field of Matter Sciences

Chemistry

Pharmaceutical Chemistry



*Final Dissertation in Master*

*Titled:*

**Physicochemical characterization and evaluation of the  
photocatalytic activity of ZnO, NiO, TiO<sub>2</sub> commercial  
oxides**

Presented by:

**Khineche Hizia**

To the Jury composed by:

*Makhloufi Rachid*

*Djani Faiçal*

*Kenouche Samir*

*M.C. « B »*

*M.C. « A »*

*M.C. « B »*

*Med Khider University- Biskra*

*Med Khider University- Biskra*

*Med Khider University- Biskra*

*President*

*Supervisor*

*Examiner*

Academic Year

2017-2018

# Acknowledgement

*First and foremost, I would like to thank **ALLAH** Almighty for giving me the strength, knowledge, ability and opportunity to undertake this dissertation and to persevere and complete it satisfactorily. Without his blessings, this achievement would not have been possible.*

*I would like to thank my thesis supervisor, **Doctor Djani Faïçal**, for her valuable guidance, encouragement and continuous optimism. You definitely provided me with the tools that I needed to choose the right direction and successfully complete my dissertation.*

*Besides my supervisor, I am very grateful to the members of the jury: **Doctor Makhloufi Rachid**, and **Doctor Kenouche Samir**. for accepting to judge this thesis.*

*Don't forgetting my teachers in all the pervious years of license and master study.*

*I would like to thank my family, especially my parents, for their encouragement, patience, and assistance over the years. Both have always expressed how proud they are of me and how much they love me. I am too proud of them and love them very much. I am grateful for them both.*

*Last, but certainly not least, I would like to thank my friends, **Sara, Amira, Wissem, Zineb, Zina, Walid, Djemaa, Sadek**, to my lovely friend my beautiful angel **Bouthaina Marzougi** for the wonderful times we shared.*

*Thank you very much, every one*

## **LIST OF TABLES**

<b>TABLE I.1</b> Basic physical properties of anatase-type Titanium dioxide	<b>6</b>
<b>TABLE I. 2</b> Principales chromophoric et auxochromic groupes.	<b>11</b>
<b>TABLE I. 3:</b> The characteristic of the colorant MB.	<b>13</b>
<b>TABLE I. 4:</b> Physical properties of Bromothymol Bleu.	<b>14</b>
<b>TABLE III.1</b> Particles sizes of different oxides	<b>39</b>
<b>TABLE III.2</b> Initial photodegradation tests of MO, MB, BB.	<b>44</b>
<b>TABLE III.4</b> The evolution of absorbance by function of concentration of ZnO and time.	<b>47</b>
<b>TABLE III.5</b> The evolution of absorbance by function of concentration of NiO and Time.	<b>48</b>

## LIST OF FIGURES

<b>FIGURE I.1.</b> Solar irradiation of $\alpha$ –terpinene [1].	<b>1</b>
<b>FIGURE,I.2.</b> Photo-fenton reactions in asolar-assisted catalytic cycle [3]	<b>2</b>
<b>FIGURE I.3.</b> Schematic illustration of basic mechanism of a solar heterogeneous photocatalytic process [5].	<b>4</b>
<b>FIGURE I.4.</b> Titanium dioxide of rutile structure and anatase presenting the lengths between atoms.	<b>6</b>
<b>FIGURE I.6.</b> Structure of orange- methyl (OME).	<b>14</b>
<b>FIGURE II.1.</b> The absorption of blue dye.	<b>18</b>
<b>FIGURE II. 2.</b> The electromagnetic spectrum indicating the ultraviolet and visible regions.	<b>19</b>
<b>FIGURE.II.3.</b> The vibrational and rotational energy levels. ....	<b>20</b>
<b>FIGURE II.4.</b> Different transitions between orbitals. ....	<b>21</b>
<b>FIGURE II.5.</b> The absorption spectrum by scanning the wavelength of the light passing through the cells [21].	<b>22</b>
<b>FIGURE II.6.</b> Principle of the powder diffractometer.	<b>25</b>
<b>FIGURE II.7.</b> Bruker-Axs Type D8 Advance diffractometer.	<b>26</b>
<b>FIGURE II.8.</b> Particles Size Distribution device (mastersizer -2000).	<b>26</b>

<b>FIGURE II.9.</b> SEM device.	<b>27</b>
<b>FIGURE II.10.</b> Device used in photodegradation.	<b>28</b>
<b>FIGURE III.1.</b> Different photocatalytic steps.	<b>32</b>
<b>FIGURE III .2.</b> FTIR spectrum of TiO <sub>2</sub> powder.	<b>33</b>
<b>FIGURE III. 3.</b> FTIR spectrum of ZnO powder.	<b>33</b>
<b>FIGURE III. 4.</b> FTIR spectrum of NiO powder.	<b>34</b>
<b>FIGURE III .5</b> XRD patterns OF TiO <sub>2</sub> .	<b>35</b>
<b>FIGURE III .6.</b> XRD patterns of ZnO.	<b>36</b>
<b>FIGURE III .7</b> XRD patterns of NiO.	<b>36</b>
<b>FIGURE III .8.</b> XRD patterns of TiO <sub>2</sub> with file ASTM (N°00-021-1272).	<b>37</b>
<b>FIGURE III .9.</b> XRD patterns of ZnO with file ASTM (N°00-036-1451).	<b>37</b>
<b>FIGURE III .10.</b> XRD patterns of NiO with file ASTM (N°00-044-1159).	<b>38</b>
<b>FIGURE III .11.</b> The Particle Size Distribution of TiO <sub>2</sub> powder.	<b>38</b>
<b>FIGURE III .12.</b> The Particle Size Distribution of NiO powder. ....	<b>39</b>
<b>FIGURE III.13.</b> SEM images of TiO <sub>2</sub> powder.	<b>40</b>
<b>FIGURE III.14.</b> SEM images of ZnO powder.	<b>40</b>

**FIGURE III.15.** SEM images of NiO powder. **42**

**FIGURE III.16.** The visible UV spectrums of MB photodegraded under the effects of TiO<sub>2</sub> concentration with time. **43**

**FIGURE III.17.** The visible UV spectrums of MB photodegraded under the effects of ZnO concentration with time. **46**

**FIGURE III.18.** The visible UV spectrums of BB photodegraded under the effects of NiO concentration with time. **47**

## TABLE OF CONTENTS

ACKNOWLEDGEMENT	I
LIST OF TABLES	II
LIST OF FIGURES	III
LIST OF CONTENTS	V
GENERAL INTRODUCTION	X

### Chapter I: Overview of Photocatalysis

I.1 INTRODUCTION	1
I.2.Principles of photocatalytic and sensitized photochemical reactions	2
I.2.1. HOMOGENEOUS PHOTOCATALYSIS	2
I.2.2. PHOTSENSITIZATION	3
I.2.3. HETEROGENEOUS PHOTOCATALYSIS	3
I.3.PRINCIPLES OF SOME PHOTOCATALYST	4
I.3.1. TITANIUM DIOXIDE	5
I.3.2. NICKEL OXIDE	8
I.3.3. ZINC OXIDE	9
I.4. OPERATING PARAMETERS IN PHOTOCATALYTIC PROCESS	9
I.5.WATER POLLUTION	10
I.5.1. USE AND APPLICATION OF DYES	12

I.5.2. NOMENCLATURE AND CLASSIFICATION	12
I.5.2.1. Methylene blue.....	13
I.5.2.2. Orange methyl.....	14
I.5.2.3. Bromothymol blue.....	14
I.6.TECHNOLOGIES USED IN WATER TREATMENT	15
I.7.APPLICATIONS OF PHOTOCATALYSIS	15
I.8.CONCLUSION	16

## **Chapter II: Characterization Techniques**

II.1.INTRODUCTION	18
II.2.UV/VISIBLE SPECTROSCOPY	18
II.3.HOW UV/VISIBLE SPECTROSCOPY WORKS	20
II.4.XRD STRUCTURAL ANALYSIS	24
II.4.1. PRINCIPLE OF OBTAINING THE SPECTRUM	24
II.5.PARTICLES SIZE DISTRIBUTION	26
II.6.SEM ANALYSIS	27
II.7.PHOTO REACTOR	28



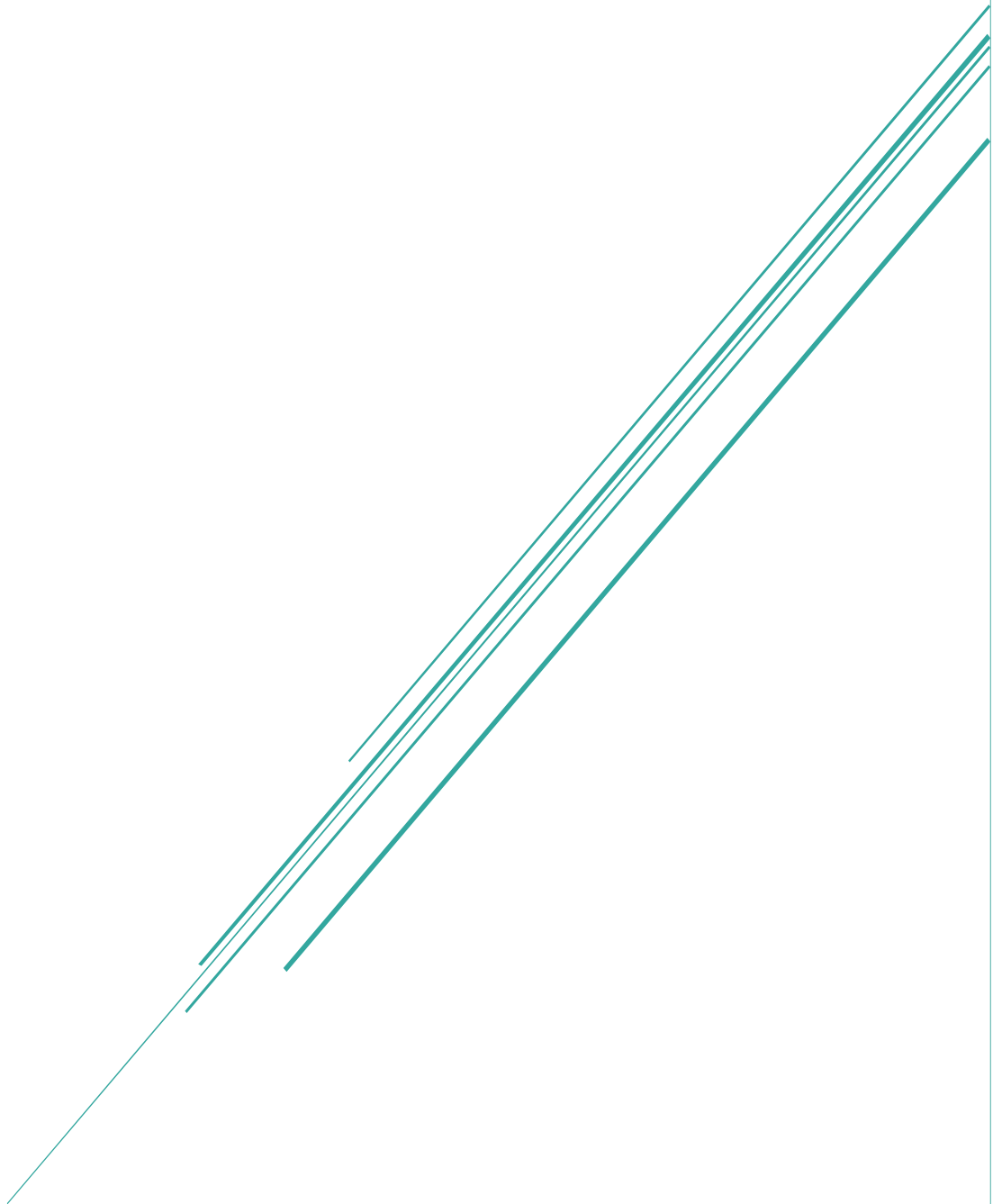
## **Chapter III: Results and Discussion**

III.1.INTRODUCTION	30
III.2.PREPARATION OF COLORANTS SOLUTIONS	30
III.3.TECHNIQUES OF CHARACTERIZATION	33
III.3.1. INFRARED (IR) CHARACTERIZATION	33
III.3.2. DIFFRACTION OF RAYONS X ANALYSIS	35
III.3.3. PARTICLES SIZE DISTRIBUTION ANALYSIS	38
III.3.4. SEM ANALYSIS	40
III.4.PHOTOCATALYTIC TEST	43
III.4.1. EFFECTS OF OXIDES CONCENTRATION (TiO <sub>2</sub> , ZnO, NiO) AND TIME	44
General conclusion	49
Abstract	51
References	47
ABREVIATION LIST	48
ANNEX	49





# Introduction



## General introduction

A photocatalyst is defined as a substance which is activated by adsorbing a photon and is capable of accelerating a reaction without being consumed [1]. These substances are invariably semiconductors. Semiconducting oxide photocatalyst have been increasingly focused in recent years due to their potential applications in solar energy conversion and environmental purification. Semiconductor heterogeneous photocatalysis has enormous potential to treat organic contaminants in water and air. This process is known as advanced oxidation process (AOP) and is suitable for the oxidation of a wide range of organic compounds. Among AOPs, heterogeneous photocatalysis have been proven to be of interest due to its efficiency in degrading recalcitrant organic compounds. Developed in the 1970s, heterogeneous photocatalytic oxidation has been given considerable attention and in the past two decades' numerous studies have been carried out on the application of heterogeneous photocatalytic oxidation process with a view to decompose and mineralize recalcitrant organic compounds. It involves the acceleration of photoreaction in the presence of a semiconductor catalyst. Several semiconductors ( $\text{TiO}_2$ ,  $\text{ZnO}$ ,  $\text{Fe}_2\text{O}_3$ ,  $\text{NiO}$ ,  $\text{CdS}$ ,  $\text{ZnS}$ ) can act as photocatalyst but some of them like ( $\text{TiO}_2$ ,  $\text{ZnO}$ ,  $\text{NiO}$ ) has been most commonly studied due to their ability to break down organic pollutants and even achieve complete mineralization. Photocatalytic and hydrophilic properties of those oxides makes them close to ideal catalysts due to their high reactivity, reduced toxicity, chemical stability and lower costs.

The main objective of this work is to characterize the physicochemical and photocatalytic properties of the following oxides  $\text{TiO}_2$ ,  $\text{ZnO}$ ,  $\text{NiO}$ .

This dissertation is organized as follow: a general introduction, three chapters and a general conclusion. The first chapter is dedicated to introduce and explain the basic concepts of Photocatalysis and semiconductor materials. In the second chapter, several characterization techniques will be presented. In the third chapter a detailed description of the steps of the work followed by the obtained results of photocatalysis using some oxides. Finally, we end with a general conclusion.



# **Overview of Photocatalysis**

**Chapter I**

## I.1. Introduction

The use of solar energy in chemical synthesis had not been explored until the beginning of the 20th century when Ciamician, called the “Father of Modern Photochemistry”, began to study the chemical behavior of organic compounds under solar irradiation. One of the first mile stones in the use of solar photochemistry was the technical-scale production of ascaridole (an anthelmintic drug) by Schenck in 1943, by solar irradiation of  $\alpha$ -terpinene.

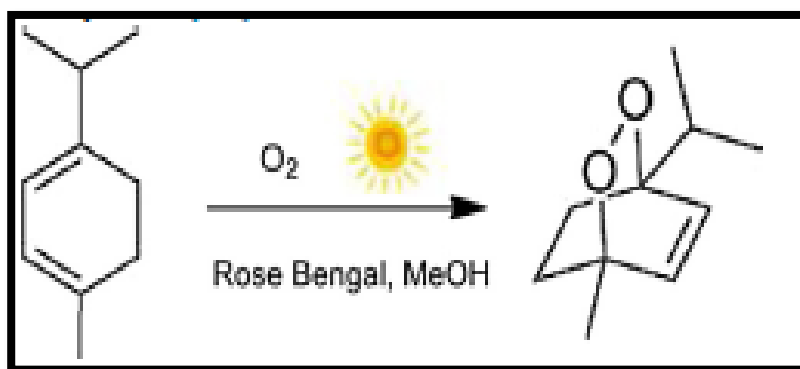


**Figure I.1.** Solar irradiation of  $\alpha$ -terpinene [1].

The first solar chemical plant, a pilot plant to produce ascaridole, was built after World War II. In the second half of the 20th century, with the development of artificial lamps, photochemistry moved indoors, during the 1970s, after the oil crisis, and influenced by growing awareness of global warming, research on the possibility of using the sunlight as an energy source was intensified, during these years, Fujishima and Honda demonstrated the market potential of heterogeneous Photocatalysis, in the wake of revival of interest in solar production, new non-concentrating and concentrating solar pilot reactors were designed and built, several experiments in solar detoxification of aqueous effluents were undertaken during the 1990s. The first experimental solar photocatalytic pilot plant, located in Albuquerque (New Mexico, USA), was designed and built in 1989 [2]. Immediately afterwards, in 1990, a similar facility was designed and built at the Platform Solar de Almeria (Almeria, Spain), since the beginning of the 21st century, applied research has also focused on the use of natural sunlight for pre-industrial fine chemical production.



## I.2. Principles of photocatalytic and sensitized photochemical reactions

The term “Photocatalysis” indicates acceleration of a photo reaction due to the presence of a catalyst [3]. This definition also takes into account photo-sensitization, a chemical process by which one molecular entity is photo-chemically altered following absorption of radiation by another molecular entity called a photo-sensitizer, however, unlike a photocatalytic process, photo-sensitization rules out photo-acceleration of a chemical reaction regardless of whether it occurs in a homogeneous or heterogeneous phase.

### I.2.1. Homogeneous Photocatalysis

The most commonly used homogeneous solar photocatalytic systems at both pilot and commercial scale are Photo-Fenton and photo-sensitized oxidation by singlet oxygen. The main Photo-Fenton reactions in a solar-assisted catalytic cycle are illustrated in the following simplified figure:

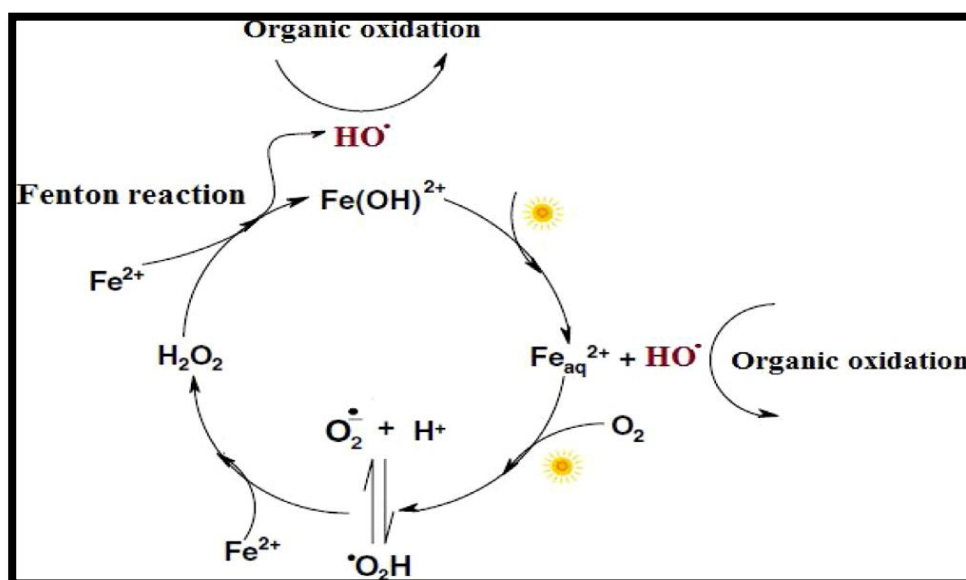


Figure I.2. Photo-Fenton reactions in a solar-assisted catalytic cycle [3].

### I.2.2. Photosensitization

Is a chemical process in which a soluble substance (sensitizer or photo-sensitizer) is capable of absorbing radiation and transferring the energy absorbed to a different reacting molecule like molecular oxygen (photo-sensitized oxidation), in this case, an oxygen molecule in the ground state ( $^3O_2$ ) is excited to a higher energy and an energized species of oxygen, singlet oxygen ( $^1O_2$ ), is formed, this unstable activated species is much more reactive than the ground triplet state and it is responsible for the selective photo-oxidation of various organic compounds to fine chemicals, since the sensitizer is not usually consumed, or at most, is only partially degraded during the photo-chemical process, returning to its original state once the reaction is complete, photosensitization may be classified as a photocatalytic reaction, methylene blue absorption wave length max, ( $\lambda_{max} = 665 \text{ nm}$ ) [4] and Rose-Bengal ( $\lambda_{max} = 550 \text{ nm}$ ) are the most popular photo-sensitizers used for the production of singlet oxygen, the homogeneous catalytic or sensitized photo-oxidation of organic substrates using sunlight as the radiation source is of increasing commercial interest in the fields of production of chemical intermediates and wastewater treatment.

### I.2.3. Heterogeneous Photocatalysis

A heterogeneous photocatalyst is a semi-conducting substance which can be chemically activated by radiation. a band model is often used for schematic representation of the electronic structures of photo semi-conducting materials, many well-documented reviews are devoted to the fundamentals of Photocatalysis in this regard, if a photo-semiconductor is irradiated by light with energy matching or greater than its band gap energy ( $E_g$ ), an electron ( $e^-$ ) in an electron-filled valence band (VB) is excited to a vacant conduction band (CB), leaving a positive hole ( $h^+$ ) in the VB. These photo-generated electrons and positive holes drive reduction and oxidation, respectively, of different compounds, not necessarily adsorbed on the surface of the photocatalyst, valence band holes ( $h^+ \text{ VB}$ ) are powerful oxidants, where, as conduction band electrons ( $e^- \text{ CB}$ ) are reductants (Figure 3), due to their electronic structures, heterogeneous photocatalyst can act as mediators in chemical redox processes, the first step is the formation of charge carriers by a photon, the excited electrons and holes in the absence of suitable electron and hole scavengers tend to

recombine very quickly, dissipating the energy as heat, photocatalytic activity is strongly dependent on the competition between the surface transfer of charge carriers and electron–hole recombination [5], if a suitable scavenger or surface defect is available to trap the photo-generated electrons or holes, recombination is limited and further.

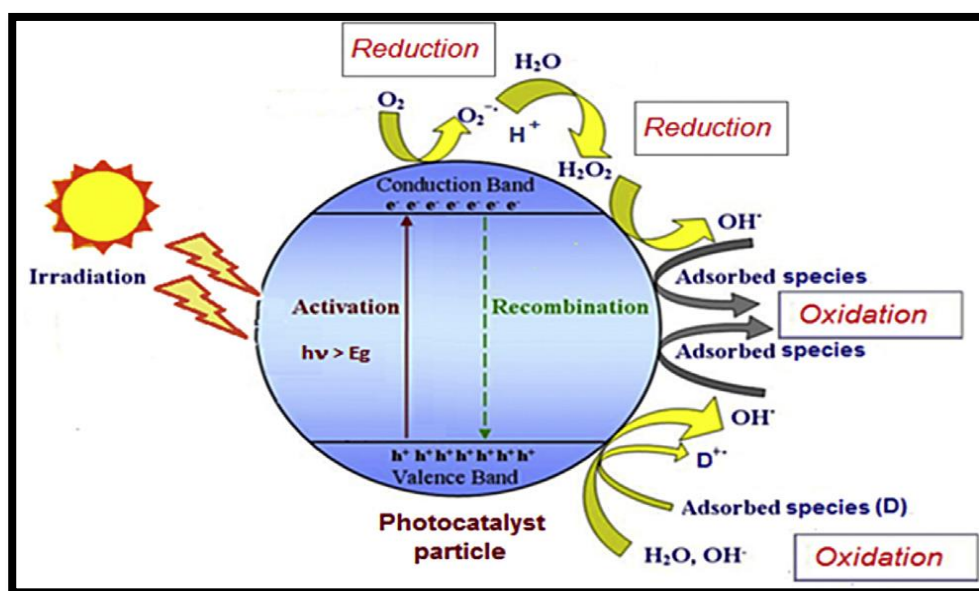


**Figure I.3.** Schematic illustration of basic mechanism of a solar heterogeneous photocatalytic process [5].

Photocatalytic reactions may occur that yield mineralization products during prolonged reaction periods, the strong oxidizing power of the positive hole can enable a one-electron oxidation step with water, normally present in the system, to produce hydroxyl radicals ( $\cdot HO$ ), which are highly reactive species able to oxidize organic molecules in liquid or gas phase, moreover, if air is also present, oxygen can act as an electron acceptor, and be reduced by the photo-electrons in the conduction band to form a superoxide ion, which is also a powerful oxidant, the width of the band gap is a measure of the strength of the chemical bond, semi-conductors that are stable under illumination, typically metal oxides, usually consist of the top of the valence band located at +3eV or lower (vs. NHE), from the stand point of solar energy, the development of photocatalyst which can drive redox reactions under visible light ( $\lambda > 400$  nm) is indispensable [6].



### I.3. Principles of Some Photocatalyst

Among the photo-semiconductors ( $\text{WO}_3$ ,  $\text{MoO}_3$ ,  $\text{ZrO}_2$ ,  $\text{SnO}_2$ ,  $\text{Fe}_2\text{O}_3$ , etc...), Titanium dioxide, mono oxide of Zinc and mono oxide of Nickel ( $\text{TiO}_2$ ,  $\text{ZnO}$ ,  $\text{NiO}$ ), are some of the most promising candidates for commercial solar applications, mainly due to their photo-chemical stability and high oxidation power, high resistance to photo-corrosion in aqueous environments, safety and lower cost than other photocatalytic materials [7].

#### I.3.1. Titanium dioxide

Titanium dioxide ( $\text{TiO}_2$ ) or titania is a very well-known and well researched material due to the stability of its chemical structure, biocompatibility, physical, optical and electrical properties. It exists in four mineral forms, as: **anatase**, **rutile**, **brookite** and titanium dioxide (B) or  $\text{TiO}_2(\text{B})$ . Anatase type  $\text{TiO}_2$  has a crystalline structure that corresponds to the tetragonal system (with dipyramidal habit) and is used mainly as a photocatalyst under UV irradiation. Rutile type  $\text{TiO}_2$  also has a tetragonal crystal structure (with prismatic habit). This type of titania is mainly used as white pigment in paint. Brookite type  $\text{TiO}_2$  has an orthorhombic crystalline structure, where anatase exhibits the highest overall photocatalytic activity, basic physical properties of the anatase-type  $\text{TiO}_2$  are listed in ( table I.1) .The highly oxidizing effect of  $\text{TiO}_2$  makes it suitable for decomposition of organic and inorganic compounds at very low concentrations ranging from 0.01 to 10 ppm , the photocatalytic effect of  $\text{TiO}_2$  can be used for self-cleaning surfaces, decomposing atmospheric pollution and self-sterilization .Titanium dioxide is a solid white substance which is handled like powder. Its purity can vary between 80 and 100%. Dominant impurities are aluminium hydroxide and silicon. The substance precipitate ( insoluble) in water.

**Table I.1** Basic physical properties of anatase-type titanium dioxide

Crystal form	Tetragonal system
Density (g/cm <sup>3</sup> )	3.90
Refractive index	2.52
Permittivity	31
Thermal stability	Change to rutile type at high temperature

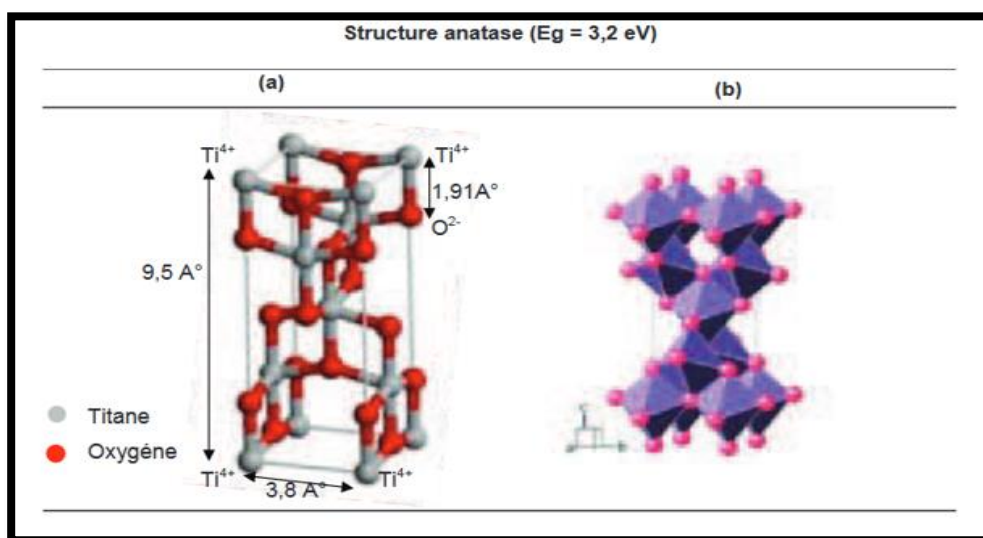


**Figure I.4.** Titanium dioxide of rutile structure and anatase presenting the lengths between atoms.

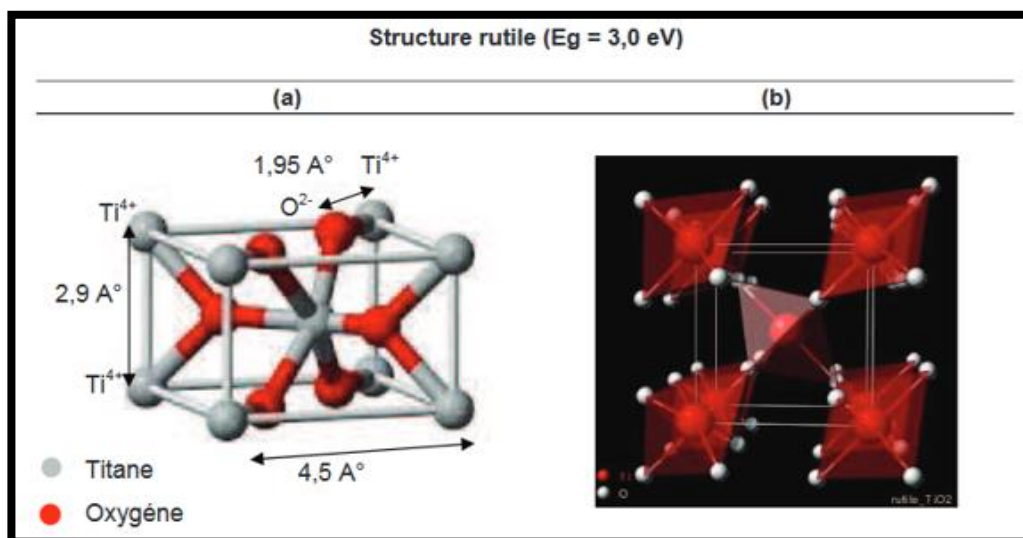


Figure I.5. Schematic structure of TiO<sub>2</sub> in anatase and rutile form.

❖ **Oxidation-Reduction Reactions**

TiO<sub>2</sub> is a semi conductive material that during illumination acts as a strong oxidizing agent lowering the activation energy for the decomposition of organic and inorganic compounds. the illumination of the surface of the TiO<sub>2</sub> induces the separation of two types of carriers:

- an electron ( $e^-$ ) and (2) a hole ( $h^+$ ), to produce these two carriers, sufficient energy must be supplied by a photon to promote an electron ( $e^-$ ) from the valence band to the conduction band, leaving a hole ( $h^+$ ) behind in the valence band. The recombination of holes and electrons is relatively slow in TiO<sub>2</sub> compared to electrically conducting materials, i.e., metals where the recombination occurs immediately:



The required energy that has to be supplied by the photons for the promotion of the electrons depends on the band gap for the specific material, the band gap is the difference in energy between the highest permitted energy level for the electron in the valence band and the lowest permitted energy level in the conduction band, the band gap is the minimum energy of light

required to make the material electrically conductive. The band gap energy,  $E_g$  of  $\text{TiO}_2$  (anatase) is 3.2 eV, which corresponds to photons with a wave length of 388 nm.

The photo induced hole can oxidize a donor molecule (D) adsorbed on the  $\text{TiO}_2$  surface.



The electron in the conduction band can reduce an acceptor molecule (A).



The strong oxidation power of the hole enables a one-electron oxidation step with water to produce a hydroxyl radical ( $\cdot\text{OH}$ ).



Oxygen can act as an electron acceptor, and be reduced by the promoted electron in the conduction band to form a super oxide ion ( $\cdot\text{O}^-$ ), the superoxide ion is a highly reactive particle, able to oxidize organic materials, the oxidation-reduction process is shown in (Figure.3).



### I.3.2. Nickel Oxide

Nickel oxide (NiO) has attracted considerable attention from those interested in the application to devices working in ultraviolet regions, with the interest specially lying in its wide band gap. It has been recorded that NiO is a cubic structured with anti-ferromagnetic and electrochromic properties. This material has important properties which are explored for several applications such as smart windows, dye sensitized photo cathode, transparent p-type semiconductors, and gas sensors. NiO thin films have been prepared by various methods such as sputtering, sol-gel, pulsed laser deposition, chemical vapor deposition, and spray pyrolysis. Among these techniques, spray pyrolysis is the widely used it is an attractive process to obtain thin films which requires low cost raw materials, adherent of deposits, very easy, safe and cheap. Furthermore, this technique leads to a large production area and it is special to give crystallized

thin films without recourse to thermal processing, on the other hand, NiO has been the subject of many research works in terms of doping. Several elements were used as a doping to improve some physical properties such as Mg, Cu, In, Li and K. [8]. Black nickel oxide or Ni<sub>2</sub>O<sub>3</sub> a black powder with Molecular Weight equal to 74.71(g/mol.) and Specific Surface Area equal to ~1.9 to 30 (m<sup>2</sup>/g).

### I.3.3. Zinc Oxide

Due to the demanding importance of titanium in the industries mentioned above, the commercialization value for TiO<sub>2</sub> have steadily increased this few years and exceeding the value of ZnO. Hence, alternative potential resources for titanium, which render the comparable efficiency, have to be considered. Among the oxide-based semiconductors that hold the promise as a potential photo-catalyst, ZnO has reflected comparable efficiency to that of TiO<sub>2</sub>, analogous to TiO<sub>2</sub>, ZnO could serve as an ideal photo-catalyst candidate that is cost-effective and due to the demanding importance of titanium in the industries mentioned above, the commercialization value for TiO<sub>2</sub> have steadily increased this few years and exceeding the value of ZnO[9], ZnO has reflected comparable efficiency to that of TiO<sub>2</sub>, analogous to TiO<sub>2</sub>, ZnO could serve as an ideal photo-catalyst candidate that is cost-effective and environment-friendly, other than that, the comparable intrinsic band gap energy of ZnO (3.37 eV) [10] to that of TiO<sub>2</sub> (3.2 eV) ,also makes it (ZnO) a suitable candidate in absorbing UV-light as an excitation source, recently, various reports have shown that ZnO are good photo-catalyst materials, for instances, (**Sakthivel et al** ) ,found that ZnO nanoparticles exhibit higher rate than that of TiO<sub>2</sub> nanoparticles ,they attributed this to the ability of ZnO in absorbing large fraction of the solar spectrum and more light quanta than that of TiO<sub>2</sub> , furthermore, have shown that photocatalytic rate efficiency of ZnO can be improved through modification of its morphology into dumbbell-shape .

### I.4. Operating parameters in photocatalytic processes

In photocatalytic degradation of dyes in wastewaters, the followings are operating parameters which affect the process as pH of the solution to be degraded, and the pH of the precursor solution (catalyst's solution during preparation of catalyst); oxidizing agent, calcination temperature, dopant content, and catalyst loading, these parameters will be considered one after



the other as they influenced the photocatalytic processes of the degradation of dyes in waste waters [13]:

- Influence of pH on photocatalytic degradation of dyes in wastewaters.
- Oxidizing agents effect on photocatalytic degradation of dyes in wastewater.
- Catalyst loading effects on photocatalytic degradation of dyes in wastewaters.
- Dopant content effect on photocatalytic activity of photocatalyst.
- calcination temperature on the activity of photocatalyst.
- Initial Concentration of Organic Compound.
- Light Intensity.
- BET surface area.

### **I.5. Water pollution**

Water is the central element of all socio-economic processes, regardless of the degree of development of society, the increase in agro-industrial activities is putting increasing pressure on the world's freshwater reserves, indeed, these activities generate a great diversity of chemicals that flow into the water cycle, jeopardizing the fragile natural balance that has allowed life to develop on the earth, often the chemicals in the wastewater are difficult to biodegrade and the lack or insufficiency of treatment systems leads to their accumulations in the water cycle, the protection of the environment has thus become an economic issue.

The contaminants that water contain are devise into five grand categories:

- a) **dissolved inorganic compounds:** constitute the majority of the impurities in water: calcium and magnesium carbonates (originally of temporary or permanent hardness sodium salts, silica from the sides of sandy rivers composed of ferrous and ferric iron from rusty channelization phosphates from nitrate detergents derived from chlorides aluminium fertilizers involved in the purification of water.
- b) **dissolved organic compounds:** come from the decomposition of plant materials (humic and fulvic acids, tannins, lignin ....), organic components from agriculture, the paper industry, household and industrial waste (detergent, grease oils, solvents, etc...) These may also be traces of detergents used in pipe cleaning. All these compounds are likely to interfere with analytical techniques and affect biological experiments.
- c) **Microorganisms and biomolecules:** microorganisms and biomolecules contaminate natural water, with bacteria being the most prevalent. chlorination applied to water systems eliminates them. [14]

**Table I. 2** Principales chromophoric et auxochromic groupes.

chromophoric groupes	auxochromic groupes
Azo (-N=N-)	Amino (-NH <sub>2</sub> )
Nitroso (-NO ou -N-OH)	Méthylamino (-NHCH <sub>3</sub> )
Carbonyl (>C=O)	Diméthylamino (-N(CH <sub>3</sub> ) <sub>2</sub> )
Vinyl (-C=C-)	Hydroxyl (-HO)
Nitro (-NO <sub>2</sub> ou =NO-OH)	Alkoxy (-OR)
Sulphure (>C=S)	électrons donor groupes

In general, the dyes consist of a group assembly chromophore, auxochromes and conjugated aromatic structures (cycles benzene, anthracene, terylene, etc.). When the number of aromatic ring increases, the conjugation of the double bonds increases and the conjugated system widens. The energy of the bonds decreases while the activity of the electrons increases and produces a shift towards the long wavelengths (bathochromic effect). Similarly, when an electron-

donating auxochrome group (amino, hydroxy, alkoxy ...) is placed on a conjugated aromatic system, this group joins the conjugation of the system, the molecule absorbs in the long wave.

### **I.5.1. Use and application of dyes**

The main areas of application of dyes are:

- In the textile industry of fur, leather (textile for clothing); decoration; building, transport, textile for medical use etc.....
- In the plastics industry (pigments).
- In the building industry: paints (pigments).
- In the pharmaceutical industry (dyes).
- In the cosmetics industry.
- In the food industry (food colors).
- In various industries used for fuels and oils.
- In printing (ink, paper).

### **I.5.2. Nomenclature and classification**

There are approximately 8000 chemically different synthetic dyes, listed in the Colors Index under 40000 trade names. The dyes are classified under a code name indicating their class, there that a serial number, according to their use, their constitutions as well as their marks [Defosse, A3 233]. The classification principles most commonly encountered in industries, are based on chemical structures of synthetic dyes and methods of application to different substrates (textiles, paper, leather, plastics, etc.).

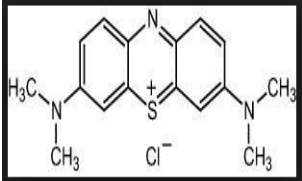
The classification of dyes according to their chemical structure is based on the nature of the group chromophore (Table I .2).

Example: Azoic dyes estimated at a production of around 350 000 tonnes per year, they are the most important family of synthetic dyes. They are characterized by the presence of the group  $-N = N-$ , and their colors is related to chromophores. According to the number of azo chromophores encountered in the molecule, we distinguish the monoazo, disazo and polyazo, [15] and other dyes like:

### I.5.2.1. Methylene blue

Methylene blue, or tetramethylthionine hydrochloride, the base of which is a base ammonium, is obtained by the action of silver oxide; this base was called **blue Borrel** by **LAVÉLAN**. It is a progressive basic dye. It belongs to the group of Quinones-imides, section Thiazines, which are dyes sulfides in which two benzene rings are united by a closed ring of a nitrogen atom, a sulfur atom and 4 carbon atoms. In this group, we will find: thionone (or Lauth violet), toluidine blue, new methylene blue (which is derived from ethyltoluidine, not dimethylaniline as his namesake; they are very close in their action!), methylene violet, methylene azure and methylene green (nitrated methylene blue). [16] night and gives darker colors.

**Table I. 3:** The characteristic of the colorant MB.

Colorants	$\lambda_{\max}$	Molar Weight (g/mol)	Chemical Structure
Methylene bleu (MB) (cationic)	663nm	373.9	

### I.5.2.2. Orange methyl

Orange methyl (OMe) ( $C_{14}H_{14}N_3SO_3Na$ ) structure is reported in (Figure 6), and characterized by sulphonic groups, which are responsible for the high solubility of these dyes in water [17].

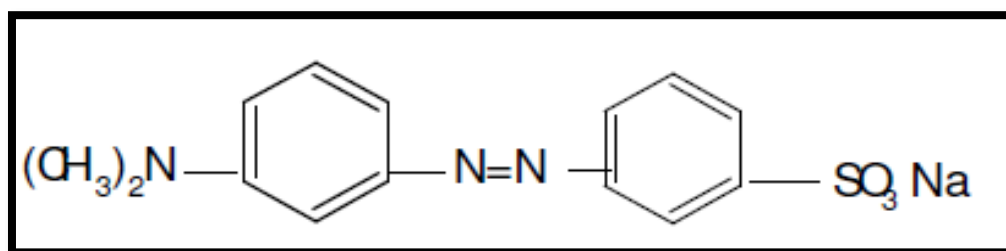


Figure I.6. Structure of Orange- Methyl (OMe).

### I.5.2.3. Bromothymol blue

Bromothymol bleu also named 3,3'-Dibromothymolsulfonphtalein or Dibromothymolsulfophthalein or named by IUPAC Thymol, 6,6'-(3H-2,1-benzoxathiol-3-ylidene) bis(2-bromo)-, S, S-dioxide is a colorant with formula  $C_{27}H_{28}Br_2O_5$  solid in the form of crystals, cream, odorless with the following physical properties in the (table I.4) [18].

Table I. 4: Physical properties of Bromothymol bleu.

Physical state	Molecular weight	Density	Solubility in water	Vapor density (air = 1)	Melting point	pH
Solid	624.39	1.25 g / ml at 20 ° C	Not very soluble	Not applicable	Not applicable	5.0% aqueous solution

## I.6. Technologies used in water treatment

One of a few attractive options is the possible reuse of onsite rural wastewater or the treated municipal wastewater from treatment plants for agricultural and industrial activities. Since these wastewaters constitute one of the largest possible water resources, its reuse is anticipated to offset more clean water resource. Recycling wastewaters are usually associated with the presence of suspended solids, health-threat coliforms and soluble refractory organic compounds that are both tedious and expensive to treat. Currently available water treatment technologies such as adsorption or coagulation merely concentrate the pollutants present by transferring them to other phases, but still remain and not being completely “eliminated” or “destroyed. Other conventional water treatment methods such as sedimentation, filtration, chemical and membrane technologies involve high operating costs and could generate toxic secondary pollutants into the ecosystem. These concentrated toxic contaminants are highly redundant and have been concerned worldwide due to the increasing environmental awareness and legislations. Chlorination has been the most commonly and widely used disinfection process. The disinfection by-products generated from chlorination are mutagenic and carcinogenic to human health. These have led to the rapid R&D in the field of “Advanced Oxidation Processes (AOPs)” as the innovative water treatment technologies. The rationales of these AOPs are based on the in-situ generation of highly reactive transitory species (i.e.  $\text{H}_2\text{O}_2$ ,  $\text{OH}$ ,  $\text{O}_2$ ,  $\text{O}_3$ ) for mineralization of refractory organic compounds, water pathogens and disinfection by-products. Among these AOPs, heterogeneous Photocatalysis employing semiconductor catalysts ( $\text{TiO}_2$ ,  $\text{ZnO}$ ...) demonstrated its efficiency in degrading a wide range of ambiguous refractory organics into readily biodegradable compounds. [19].

## I.7. Photocatalysis applications

the applications of Photocatalysis are numerous and the object of this paragraph is not to make it an exhaustive list but simply to give an idea of the many perspectives offered by this process:

- Hydrogen production.
- Use of solar radiation.
- Fine chemistry.
- Decontamination.

- Air and water treatment,
- Self-cleaning materials etc.....

Are all tracks currently explored by researchers in the field of Photocatalysis. Finally, we can't talk about the applications of Photocatalysis without mentioning the case, degradation of the pollutants of the air and water. the treatment of effluents by photocalytic oxidation is actually one of the strong points of the process today since many industrial applications derive there from. [20]

## **I.8. Conclusion**

Semiconductor Photocatalysis appears to be a promising technology that has a number of applications in environmental systems such as air purification, water disinfection, hazardous waste remediation, and water purification. In addition, the basic research that underlies the application of this technology is forging a new understanding of the complex heterogeneous photochemistry of metal oxide systems in multiphasic environments.

# Characterization Techniques

## Chapter II



## II.1. Introduction

Many efficient techniques were developed for preparation of nanostructures oxides, mainly including sol-gel, precipitation, sonochemical thermal decomposition, microwave, water-in-oil micro emulsions and so on. Recently, the sublimation method as a novel route has been developed to synthesize organometallic compounds in Nano-scale that are used as precursors for synthesis of metal oxide compounds by thermal decomposition. This process is simple and eco-friendly due to its properties such as low-temperature of the reaction and free-solvent, as well as, using precursor in nano-scale is an advantage of it. In this work, we used prepared oxides (from market) but there is some ways (methods) to prepare such oxides, we are interested in the most common in giving some examples of techniques used to form oxides whose properties are particularly interesting. In this chapter we will going to present the experimental techniques used in this work, those techniques are used to characterize the structure and properties such as XDR X-ray diffraction, Infrared IR, UV visible, laser granulometry, Scanning electron microscopy SEM.

## II.2. UV/visible spectroscopy

The absorption of light is familiar to everyone. The absorption of visible light is what makes things colored. For example, a blue dye used in a pair of jeans appears blue because the light at the red end of the spectrum is absorbed. This leaves the blue light to be reflected to the observer's eye (Figure.II.1). Ultraviolet:  $200 \leq \lambda \leq 400\text{nm}$  Visible:  $400 \leq \lambda \leq 800\text{nm}$ .

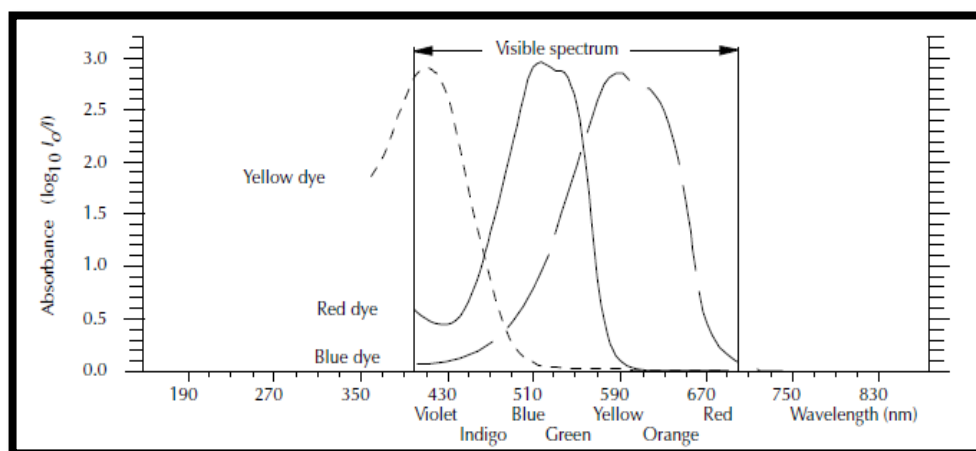


**Figure II.1.** The absorption of blue dye.

Ultraviolet/visible spectroscopy is useful as an analytical technique for two reasons. First it can be used to identify some functional groups in molecules and secondly, it can be used for assaying. This second role – determining the content and strength of a substance – is extremely useful. Ultraviolet/visible spectroscopy is used extensively in chemical and biochemical laboratories, for a variety of tasks. It can be used to determine small quantities such as the trace metal content in alloys or the amount of a certain drug reaching various parts of the body. The optical whiteners used in washing and detergent powders and toothpaste absorb ultraviolet/visible light to good effect. The whitener absorbs radiation in the near ultraviolet and then emits it in the visible range. Consequently, if you have ever been to a nightclub and have seen a white shirt appear purple/blue under ultraviolet light this is why. It is also the reason why people with false teeth should not smile! An increasingly important use of the absorption of ultraviolet/visible light is the coding of household items with ultraviolet sensitive ink and using invisible – but ultraviolet fluorescent – inks for signatures in building society savings books. (Figure.II.2) shows the electromagnetic spectrum indicating the ultraviolet and visible regions.

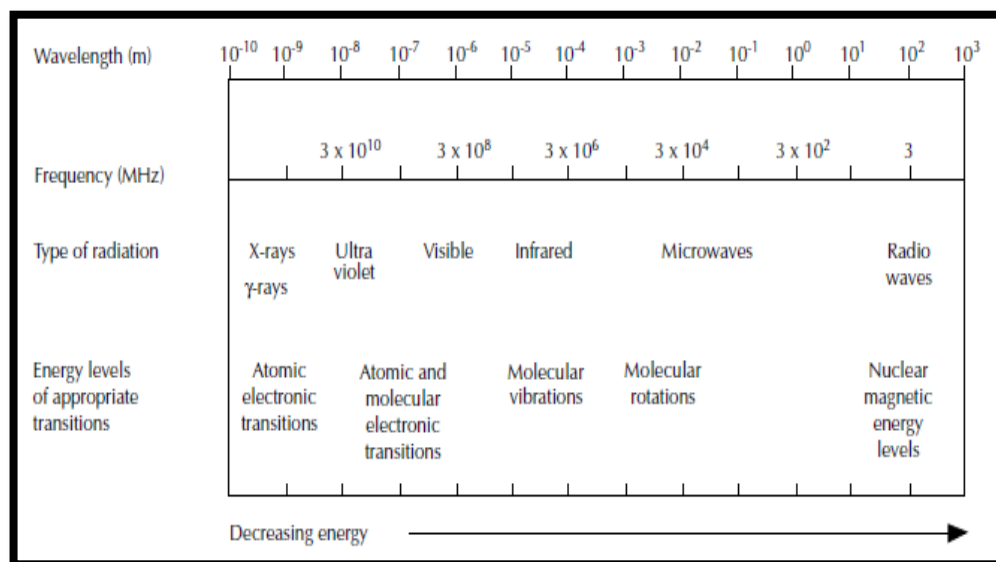


**Figure II. 2.** The electromagnetic spectrum indicating the ultraviolet and visible regions.

### II.3. How UV/visible spectroscopy works

When light – either visible or ultraviolet – is absorbed by valence (outer) electrons these electrons are promoted from their normal (ground) states to higher energy (excited) states (*Figure.II.3*). The energies of the orbitals involved in electronic transitions have fixed values. Because energy is quantized, it seems safe to assume that absorption peaks in a UV visible

spectrum will be sharp peaks. However, this is rarely, if ever, observed. Instead the spectrum has broad peaks (*Figure.II.5*). This is because there are also vibrational and rotational energy levels available to absorbing materials (*Figure.II.3*).

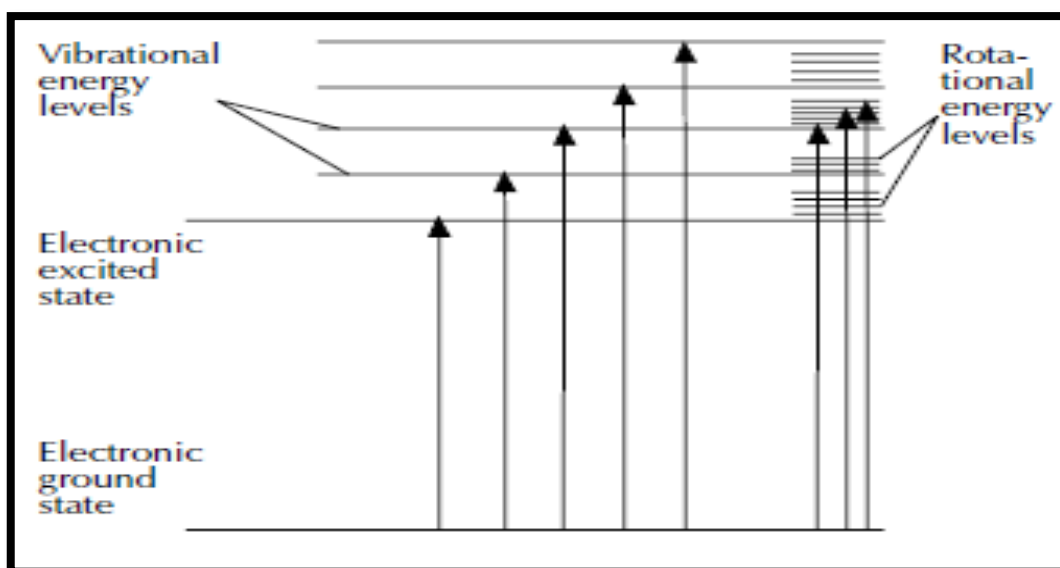


**Figure.II.3.** The vibrational and rotational energy levels.

Because light absorption can occur over a wide range, light from 190 nm to 900 nm is usually used. So how is the absorption of light explained? Valence electrons are found in three types of electron orbitals. Single, or  $\sigma$ , bonding orbitals; double or triple ( $\pi$  bonding orbitals); and non-bonding orbitals (lone pair electrons). Sigma ( $\sigma$ ) bonding orbitals tend to be lower in energy than  $\pi$  bonding orbitals, which in turn are lower in energy than non-bonding orbitals. When electromagnetic radiation of the correct frequency is absorbed a transition occurs from one of these orbitals to an empty orbital, usually an antibonding orbital –  $\sigma^*$  or  $\pi^*$  – (*Figure. II. 4*). Most of the

transitions from bonding orbitals are too high a frequency (too short a wavelength to measure easily), so most of the absorptions involve only  $\pi \rightarrow \pi^*$ ,  $n \rightarrow \sigma^*$  and  $n \rightarrow \pi^*$  transitions.

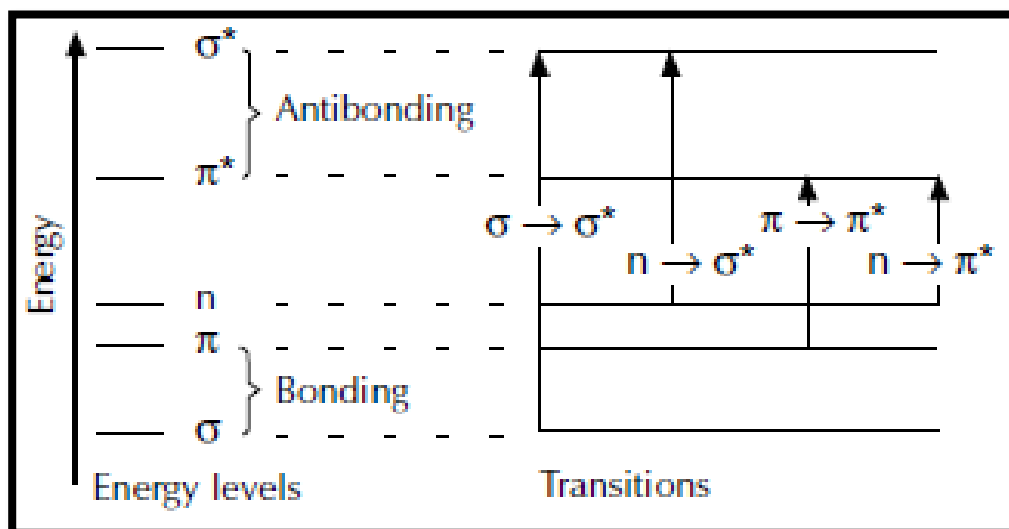


**Figure II.4.** different transitions between orbitals.

The exact energy differences between orbitals varies. In organic molecules double bonds which are next to each other can conjugate – join together and delocalize the electrons over all of the atoms. This lowers the energy needed to promote the outer electrons. As a consequence, molecules with many conjugated double bonds can be colored because they absorb energy in the visible as well as the ultraviolet part of the spectrum.

### ❖ The spectrometer

Samples are used in solution and are placed in a small silica cell. Two lamps are used. A hydrogen or deuterium lamp for the ultraviolet region and a tungsten/halogen lamp for the visible region. In this way radiation across the whole range is scanned by the spectrometer.

A reference cell containing only solvent is used. Light is passed simultaneously through the sample cell and reference cell. The spectrometer compares the light passing through the sample with that passing through the reference cell. The transmitted radiation is detected and the spectrometer records the absorption spectrum by scanning the wavelength of the light passing through the cells. A schematic diagram is shown in (Figure. II. 5). Single beam instruments are

now available as well as double beam instruments. Radiation across the whole range is monitored simultaneously.

The principles are the same as for double beam instruments, but data on the reference are taken first, followed by the sample. In this way single beam instruments can record the spectrum very quickly. [21]

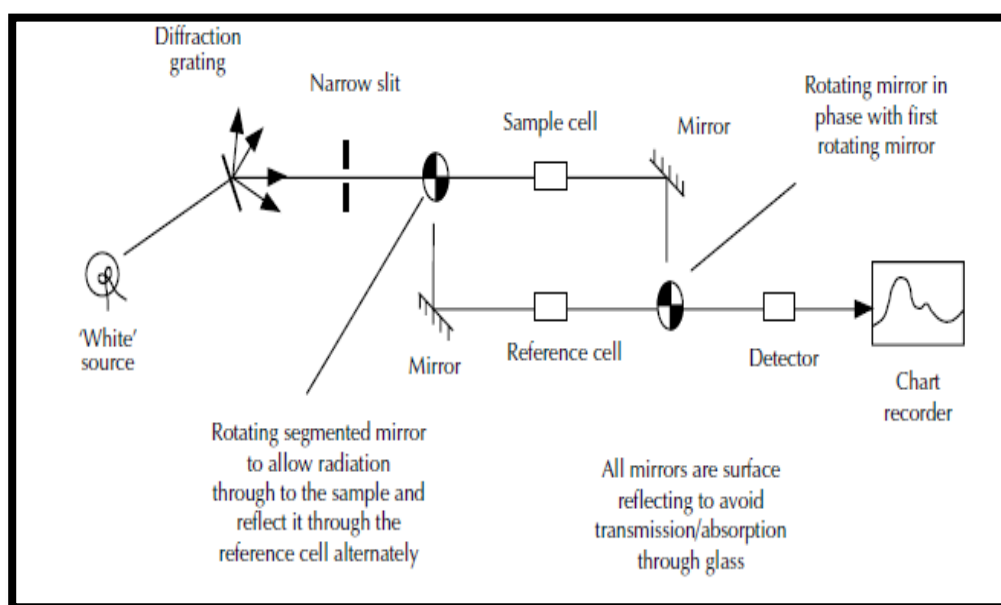


**Figure II.5.** The absorption spectrum by scanning the wavelength of the light passing through the cells [21].

### ❖ Absorption Law

At a given wavelength, absorption is proportional to the concentration of absorbing molecules and the path length of the light through the sample.

**Beer–Lambert law:**

$$A = \log_{10}(I_0/I) = \epsilon \cdot c \cdot l \quad (\text{eq II.1})$$

**A** = absorbance of the sample =  $\log_{10}(I_0/I)$

**I<sub>0</sub>** = intensity of the radiation entering the sample

**I** = intensity of the radiation emerging from the sample

$L$  = length of the light path through the sample, in centimeters

$c$  = concentration of the sample, in moles/liter

$\epsilon$  = molar absorptivity ( $L \cdot mol^{-1} \cdot cm^{-1}$  or  $M^{-1} \cdot cm^{-1}$ ) where  $M = mol \cdot L^{-1}$

The molar absorptivity (formerly called the extinction coefficient) of a compound is a constant that is characteristic of the compound at a particular wavelength

Molar absorptivities may be very large for strongly absorbing compounds ( $>10,000$ ) and very small if absorption is weak ( $= 10$  to  $100$ ). No absorption gives  $e = 0$ !

the samples are dissolved in solvents which do not absorb in the spectral region under examination (ethanol, methanol, cyclohexane).

- A source or sources of light: white light for measurement in the visible spectrum (polychromatic light) and / or UV light. The UV lamp is usually of the deuterium type, the visible lamp is generally of the halogen type, there are also spectrophotometers with a lamp xenon.
- A monochromator formed of a network diffracting the light of the source. It allows to select the wavelength of the light which will cross the studied solution.
- A slot of fixed or variable width to adjust the bandwidth.
- A tank holder that can maintain the desired temperature of the reaction depends on the solution to be analyzed, this temperature is maintained by a water circuit or a Peltier effect. This maintain fixed temperature is very useful in kinetic measurements (the speed of the reaction depends on temperature).
- A transparent tank in which the solution to be studied. Next the quality and the quantity sample, there are various tanks, generally in plastic (visible spectrum. UV close) or in quartz (UV).

Since the solvent used is not always transparent, it is obligatory to make a "blank" or compensation indicator, i.e. one to zero of the device, by placing only the solvent used in the carbon before the first measurement and this for each studied wavelength.

## II.4. XRD Structural analysis

X-ray powder diffraction (XRD) analysis is a convenient method for identify, differentiate the various phases of a mixture and determine their domain of existence. Sample preparation seems to be one of the essential parameters for obtaining reproducible results and good qualities, because the four pieces of information The main results obtained from the diffraction data are influenced by the sample:

- ❖ The position of the lines.
- ❖ The intensity of the lines.
- ❖ The shape of the lines.
- ❖ The continuous background.

### II.4.1.Principle of obtaining the spectrum

The powder, consisting of an infinity of grains (crystallites), is bombarded by a monochromatic x-ray beam of known wavelength produced by an anticathode of copper. The emitted radiation is defined by a system of slots (slots Soller) and windows (barriers) located before and after the sample. The latter is placed on a door sample that rotates uniformly around an axis in its plane (goniometric circle), thus increasing the number of possible orientations reticular planes (hkl). The particles being randomly oriented, there will always be a family of giving planes places to diffraction, i.e. for which the relation of **BRAGG** is verified.

$$\text{➤ } 2 dhkl \sin \theta = n \lambda \quad (\text{eq II.2})$$

- $\lambda$ : Wavelength of the incident X-ray beam.
- $\theta$ : Diffraction angle.
- **dhkl**: inter-sectional distance characterizing the family of planes identified by indices h, k, l.
- **n**: integer.

A detector measures the intensity of the (X) radiation diffracted in some directions. It revolves around the same axis but at a speed twice that of the sample. For an angle of incidence

( $\theta$ ), the angle measured by the displacement of the counter will be ( $2\theta$ ). A knife diaphragm eliminates the parasitic effect of incident beam in small angles ( $2\theta < 10^\circ$ ). The diffracted ray is transmitted under signal form which is amplified and recorded as a diagram  $I = f(2\theta)$ , (Figure.II.6).

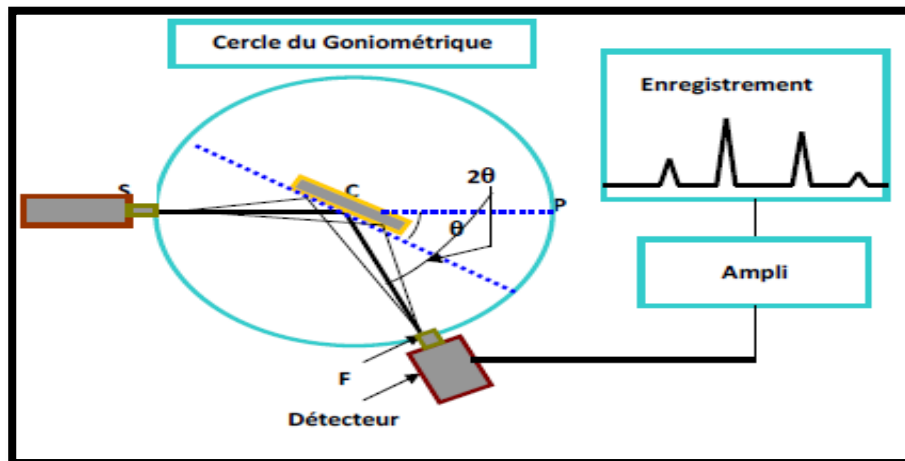


**Figure II.6.** Principle of the powder diffractometer.

The acquisition is carried out by a control unit and the processing of diffractograms where spectrum is performed using data-driven software American Society for Testing and Materials (ASTM) files, correspond the interticular distances ( $d$ ) to the recorded angles ( $2\theta$ ). The position of diffraction peaks allows the identification of structures or crystalline phases present in the sample analyzed. It should be noted that the powder must be finely ground to obtain an exploitable diagram.

The spectrum of our powders are made at room temperature on a vertical diffractometer, "BRUKER-AX type D8" (Figure II.9) in the X-ray laboratory of the University of Biskra. This last works by using  $K\alpha$  radiation from copper ( $\lambda_{K\alpha 1} = 1.541838 \text{ \AA}$ ), and it works under a high voltage of 40 KV and a current of 40 mA. Line profiles were measured using an automatic counting system point by point with a pitch of  $0.02^\circ$ . All diffraction patterns are recorded in the angular domains  $10^\circ < 2\theta < 90^\circ$ , which seem to be sufficient for the identification of the different phases [22].





Figure II.7. BRUKER-AXS type D8 ADVANCE diffractometer.

## II.5. Particles Size Distribution

The Particles size distribution makes it possible to assess quantitatively the distribution granulometry of the powders. The measurement technique is based on different types interactions between particles and Laser radiation. The apparatus used is a **Malvern-Mastersizer 2000- Hydro 2000G** (Figure II.8). This device measures particle sizes in the range 0.02 to 2000 $\mu\text{m}$ . The measurements are carried out in an aqueous medium (added water of sodium hexa metaphosphate (dispersant)) after deagglomeration of the powders by ultrasound for 15 minutes.

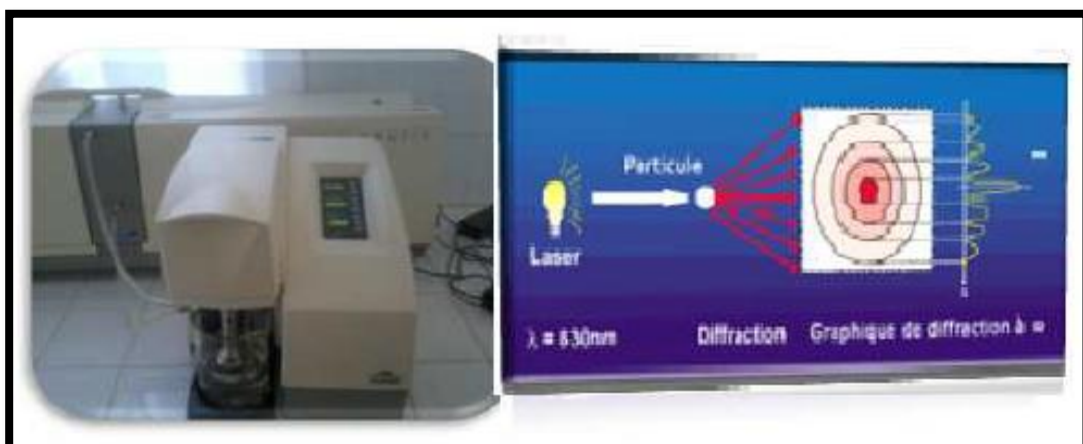
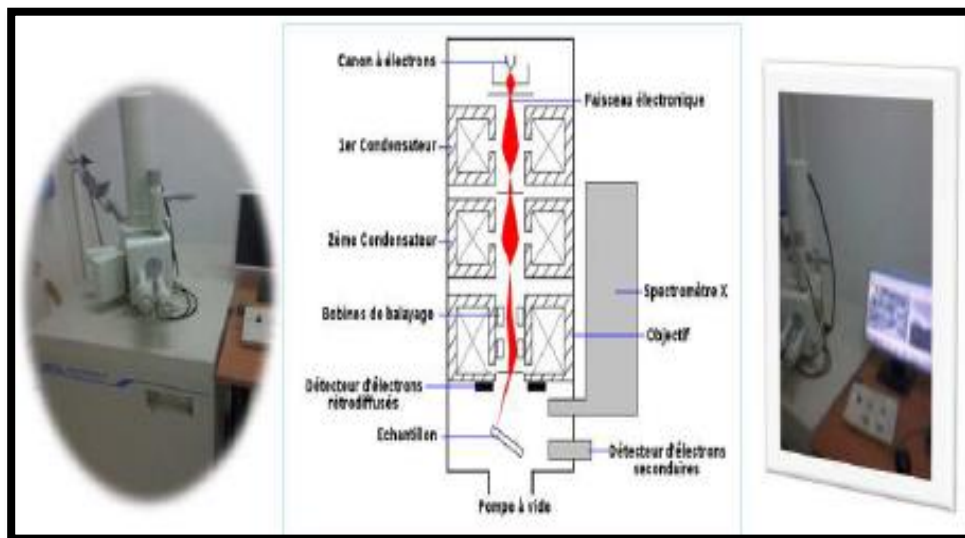


Figure II.8. Particles Size Distribution device (Mastersizer -2000).

The granulometric measurements are carried out for our pure products in using a Malvern-Mastersizer 2000-Hydro 2000G type laser scattering granulometer. The powder is suspended in 600ml of water by adding 0.6g of sodium hexametaphosphate (dispersant) and is ultrasonically dispersed for 15minutes. This device measures particle sizes in the range 0.02 to 2000  $\mu\text{m}$ . [23].

## II.6. SEM analysis:

Scanning electron microscopy (SEM) analysis makes it possible to obtain a topological or chemical image of the sample. It's a technique based on detection secondary electrons harvested by bombardment of the sample (Figure II.11). An electron beam scans the surface of the sample, and the reflected electrons are collected by a detector, the signal thus obtained is transformed into a light spot on the screen of a cathode ray tube; the brilliance of this point depends on the intensity of the signal detected, and its position on the screen corresponds to that of the point hit by the beam of electrons.



**Figure II.9.** SEM device.

Scanning electron microscopy provides information on the shape and grain size. This technique makes it possible to estimate the particle size distribution, the size grain after heat treatment and qualitatively evaluate the presence porosity or parasitic phase. The micrographs of

our sintered samples are made at using a JEOL JSM -6390LV type microscope from the X-ray laboratory of University of Biskra. It is computer controlled by operating software.

### II.7. Photo reactor

In our study we used a photo reactor with a stirring system and lamps with different light energies. a photo reactor is a device consisting of a closed system of Aluminum, based on the exposure of the light, which is the most important factor for the photocatalytic reaction to be carried out, and a stirring system for the homogeneity of the products used.



**Figure II.10.** device used in photodegradation.

# Results and Discussion

**Chapter III**

### III.1. Introduction

the objective of this chapter is to characterize the photocatalytic properties of some oxides using different techniques such as X-ray diffraction (XRD), Infrared IR, (SEM) Scanning Electron Microscopy, Particle Size Distribution (PSD), UV visible.

### III.2. Preparation of colorants solutions

✓ **synthesis protocol:**

The solutions of the different colorants are prepared, 0.005 g of orange methyl dissolved in 500 ml of distilled water are taken, and 0.0479 g of bromothymol blue dissolved in 1000 ml of distilled water is also taken.

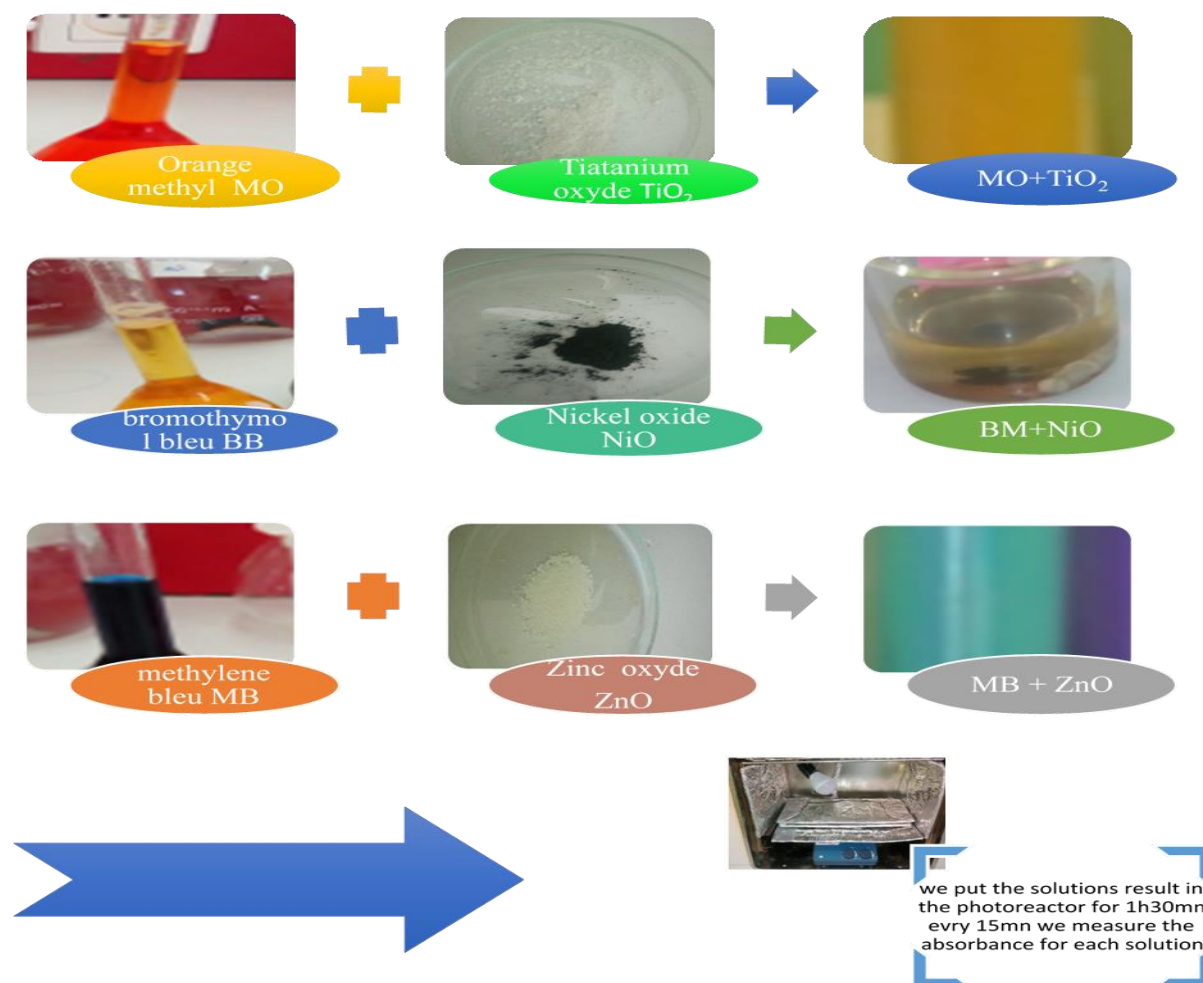
the resulting solutions are left stirring at room temperature until the complete dissolution of products in the absence of light, we take a quantity from its solutions and put it in the light and after 24h the absorbance is measured.

✓ **Dissolution of mixtures**



✓ Protocol of synthesis

The product used are Methylene bleu, Methyl-Orange( $C_{14}H_{14}N_3SO_3Na$ ), Bromothymol bleu ( $C_{27}H_{28}Br_2O_5$ ) dissolute in water as solvent. We take every time 20ml of the solution of MO and we put 0.5mg,1mg,2mg of  $TiO_2$  respectively. Also we did the same work for : NiO with BB and ZnO with MB



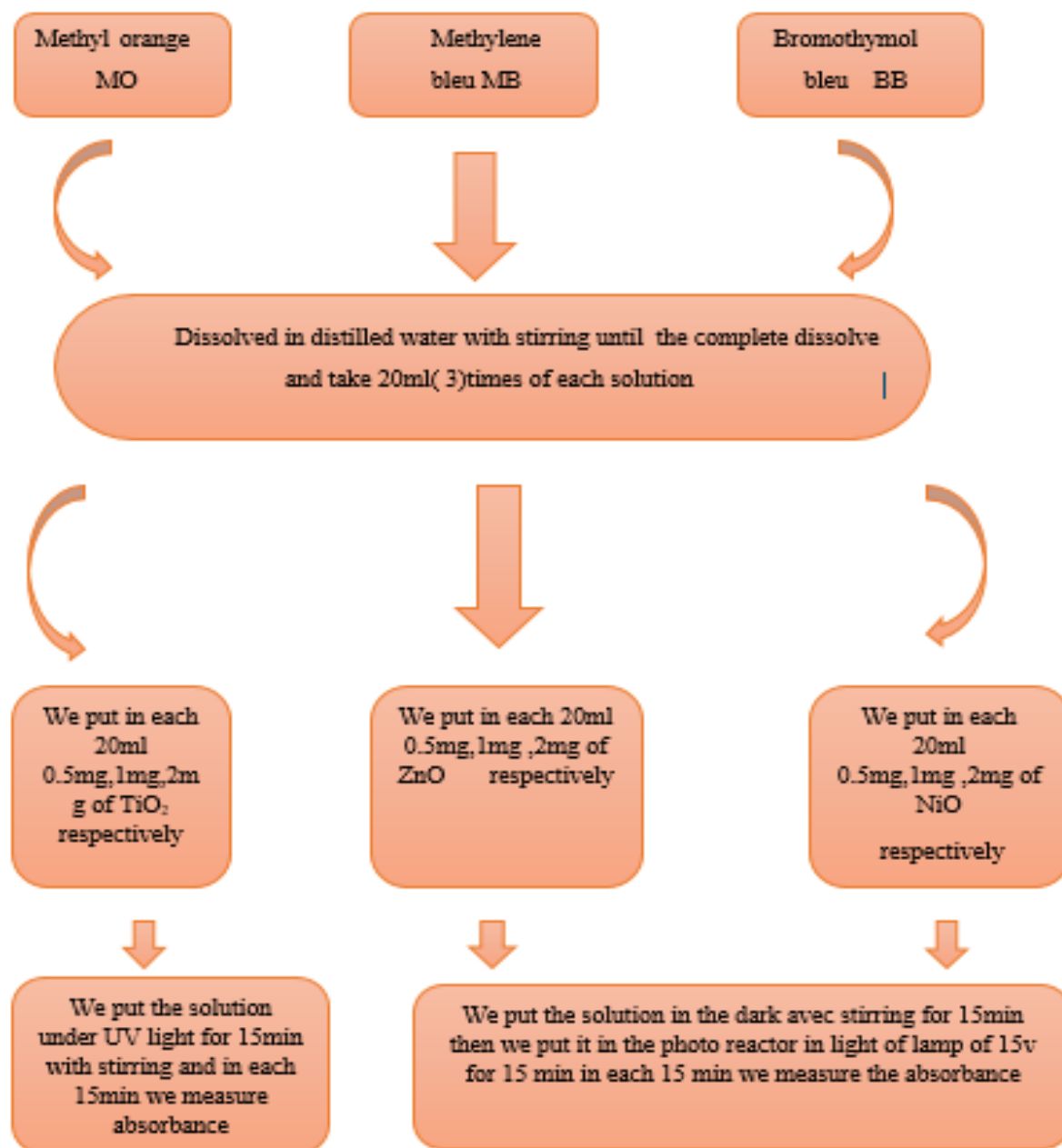


Figure III.1. different photocatalytic steps.

### III.3. Characterization techniques

#### III.3.1. Infrared (IR) Characterization

The infrared analyses of the substances make it possible to highlight the different functional groups present, for our study the infrared spectra in transmission were realized on a spectrometer transformed of fourier of type, the wavelengths studied are between 4000-400  $\text{cm}^{-1}$  analysis at was carried out on the three samples  $\text{TiO}_2$ ,  $\text{ZnO}$ ,  $\text{NiO}$  FT-IR spectrum of sample number 1 is shown in (Figure 2). This spectrum shows an absorption band at 886  $\text{cm}^{-1}$ , which may be assigned to the Ti-O stretching vibration mode. The interaction of the metal with oxygen and resonance in ligand that this resonance is confirmed by the C=O weak peak at 1460  $\text{cm}^{-1}$ .

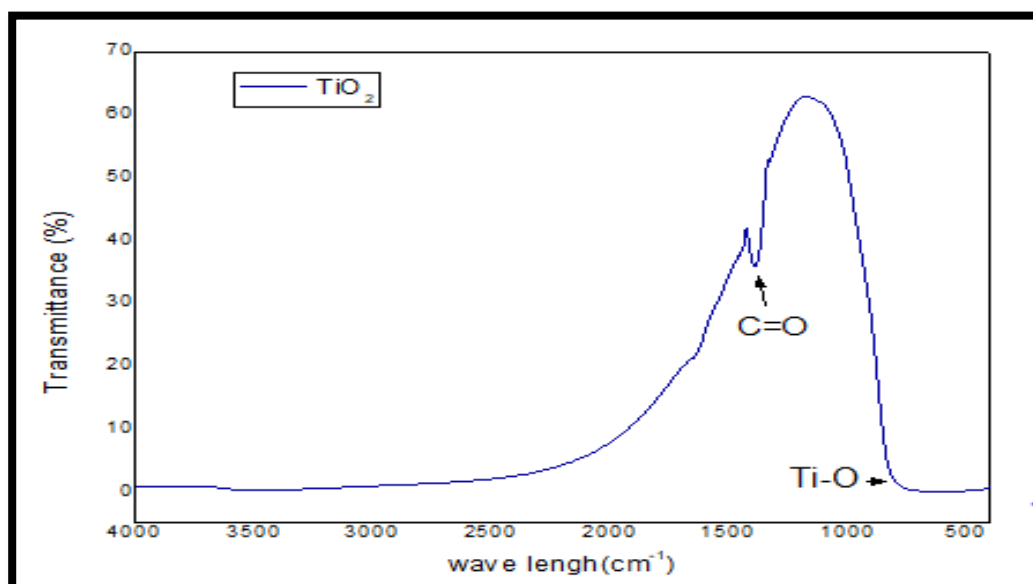
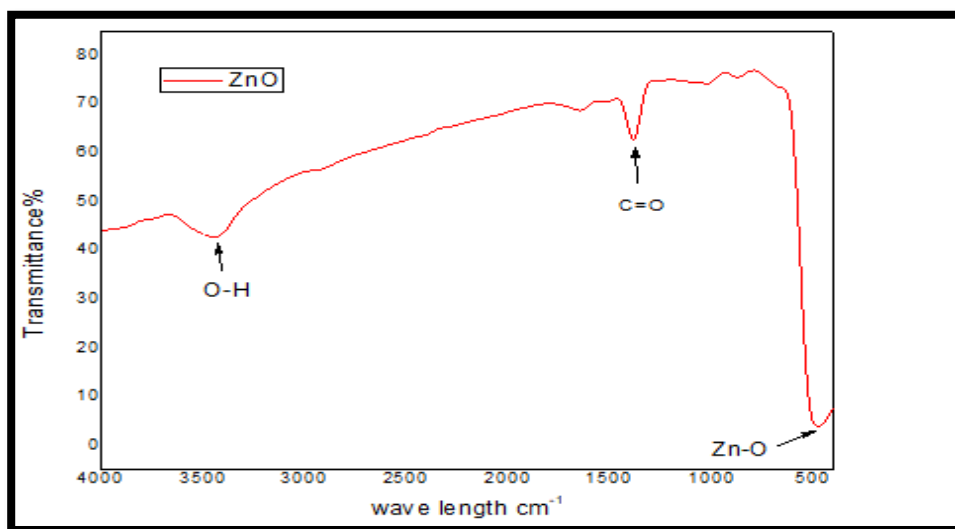


Figure III .2. FTIR Spectrum of  $\text{TiO}_2$  powder.





**Figure III. 3.** FTIR Spectrum of ZnO powder.

FT-IR spectrum of sample number 2 is shown in (Figure 3). This spectrum shows an absorption band at  $596\text{ cm}^{-1}$ , which may be assigned to the Zn -O stretching vibration mode. The interaction of the metal with oxygen and resonance in ligand that this resonance is confirmed by the C=O weak peak at  $1483\text{ cm}^{-1}$ . The broad absorption band around  $3496\text{ cm}^{-1}$  is corresponding to the  $\nu(\text{O-H})$  stretching vibrations of water molecules adsorbed on the surface of ZnO.

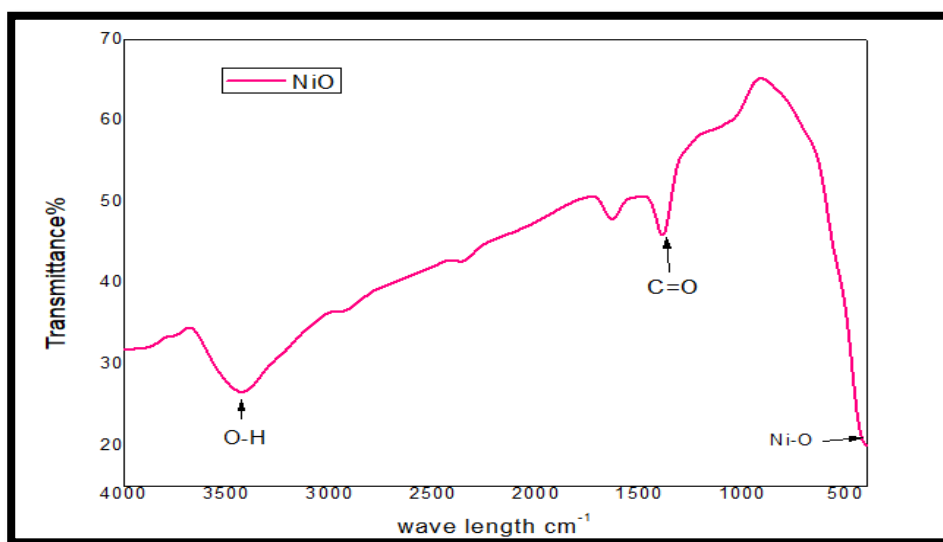


**Figure III. 4** FTIR Spectrum of NiO powder.

FT-IR spectrum of sample number 3 is shown in (Figure. 4). This spectrum shows an absorption band at  $460\text{ cm}^{-1}$ , which may be assigned to the Ni -O vibration mode. The important peak at  $1554\text{ cm}^{-1}$  in the spectrum, correspond to mode stretching  $\text{C}=\text{O}$  and the shifting of carbonyl group peak is due to the interaction of the metal with oxygen and resonance in ligand that this resonance is confirmed by the  $\text{C}=\text{O}$  weak peak at  $1475\text{ cm}^{-1}$ . The weak peak at  $2942\text{ cm}^{-1}$  corresponding to methyl and methylene groups asymmetric stretching vibrations. The broad absorption band around  $3450\text{ cm}^{-1}$  is corresponding to the  $\nu(\text{O-H})$  stretching vibrations of water molecules adsorbed on the surface of NiO nanostructure.

### III.3.2. Diffraction of rayons X Analysis

The X-ray diffractogram (figure 5) shows the presence of the two phases crystalline anatase and rutile, whose main diffraction angles in  $2\theta$  are  $25.3^\circ$ ;  $37.8^\circ$  and  $48, 1^\circ$  for the anatase and  $27.4^\circ$ ;  $36.1^\circ$  and  $56.4^\circ$  for rutile.

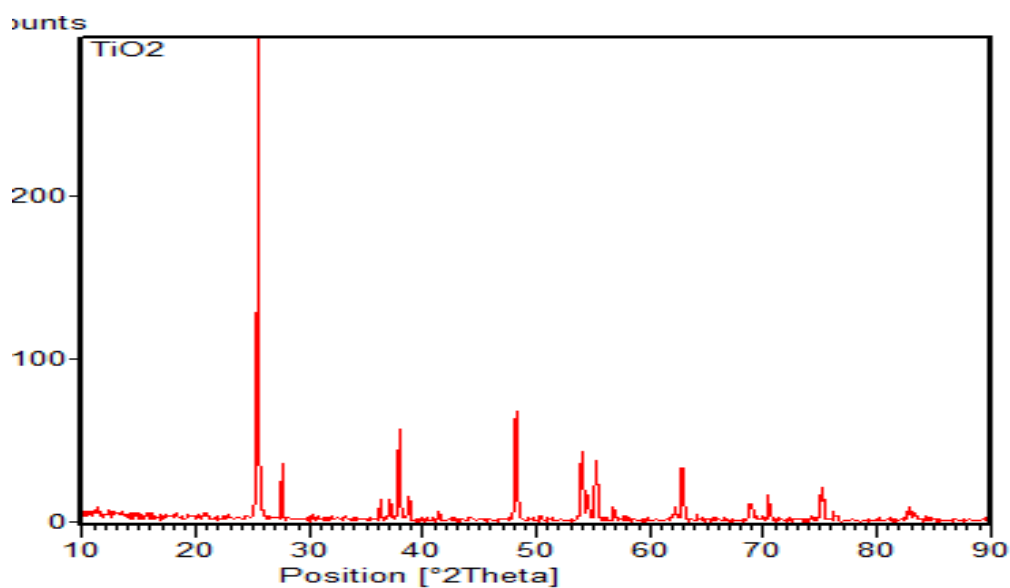
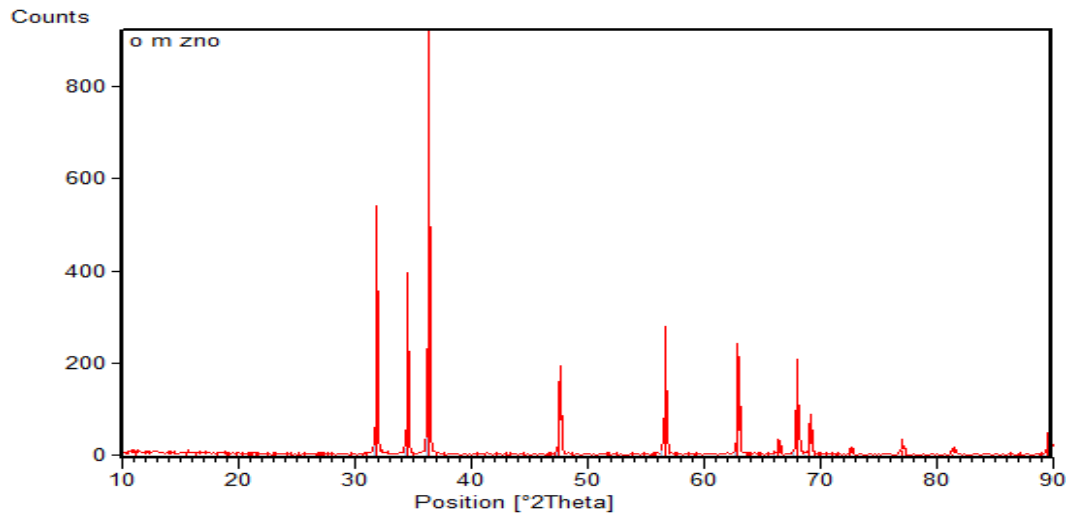
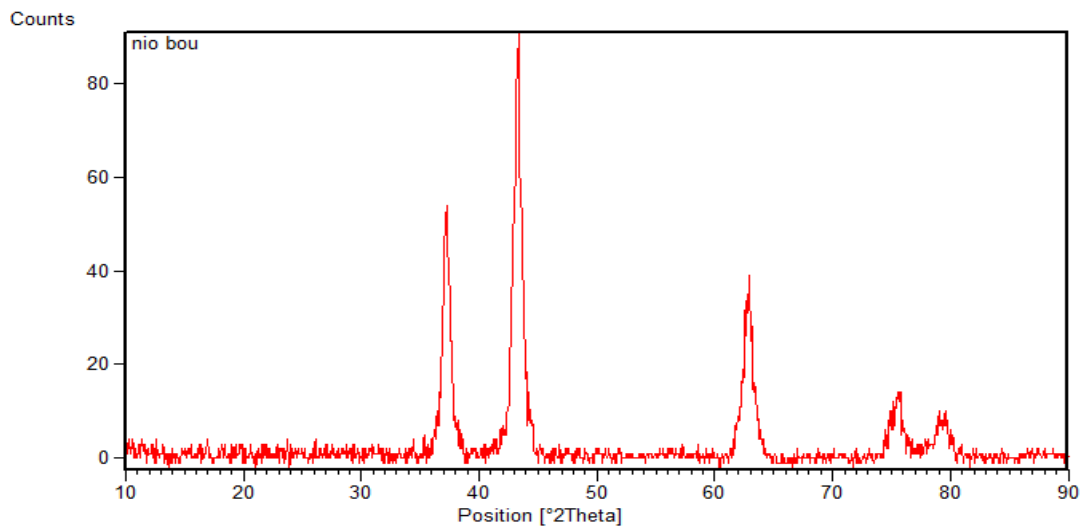


Figure III .5. XRD patterns of TiO<sub>2</sub>



**Figure III .6.** XRD patterns of ZnO

The X-ray diffractogram (6) shows Zincite, syn common name is Chinese white.



**Figure III .7.** XRD patterns of NiO

The X-ray diffractogram (7) , shows NiO with Crystal system Rhombohedral

The following figures show a comparison of the diffractograms of the different oxides and with an ASTM file of the same type of compound used.

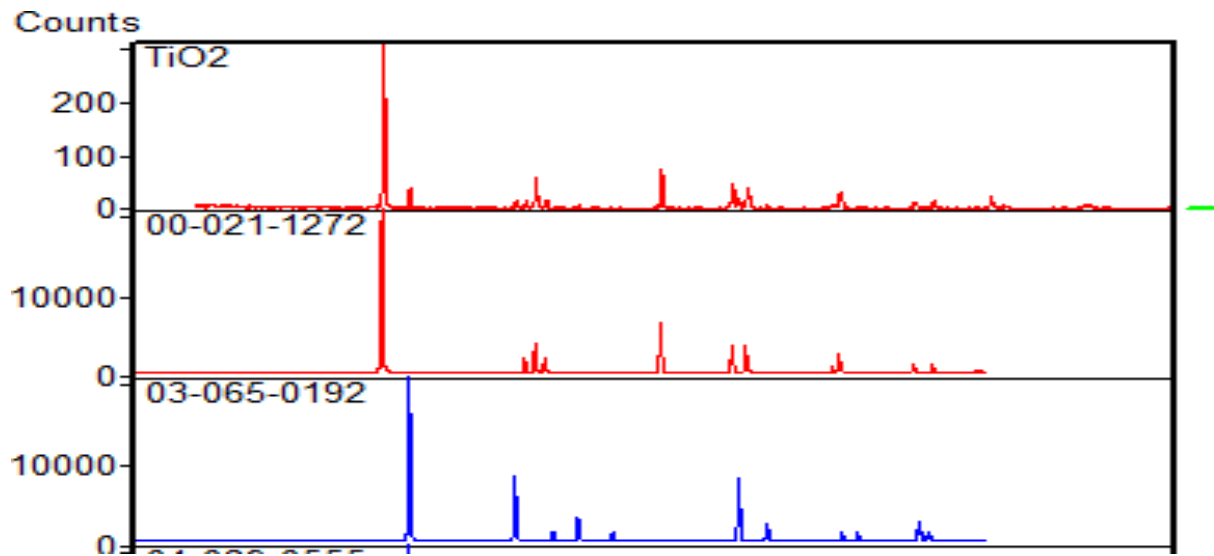


Figure III .8. XRD patterns of TiO<sub>2</sub> with file ASTM (N°00-021-1272)

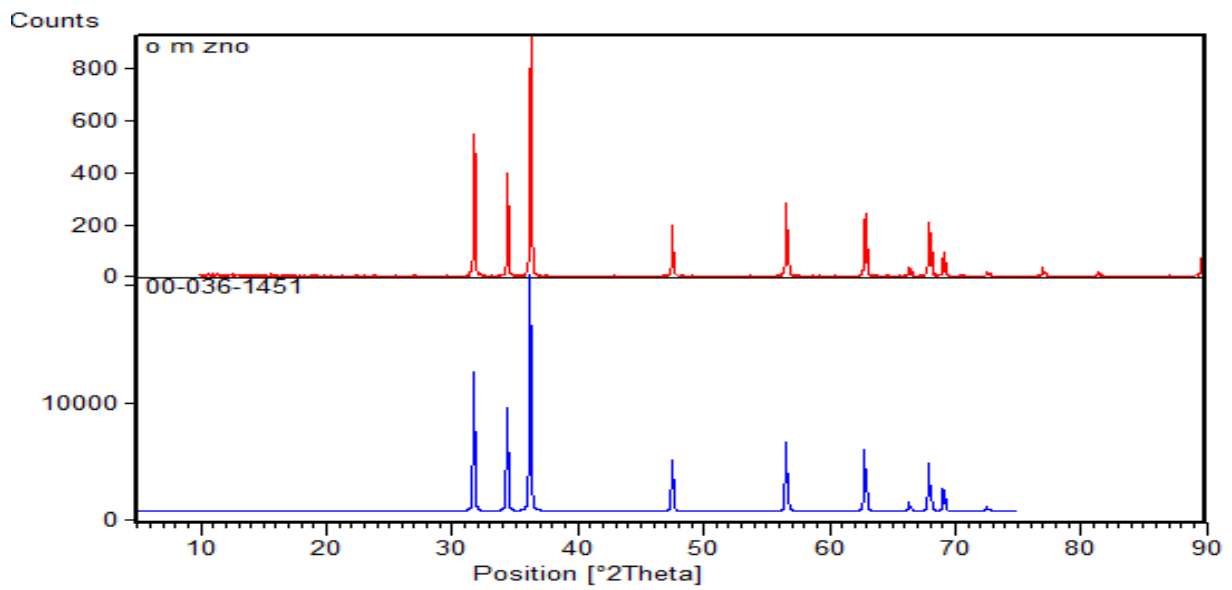


Figure III .9. XRD patterns of ZnO with file ASTM (N°00-036-1451)

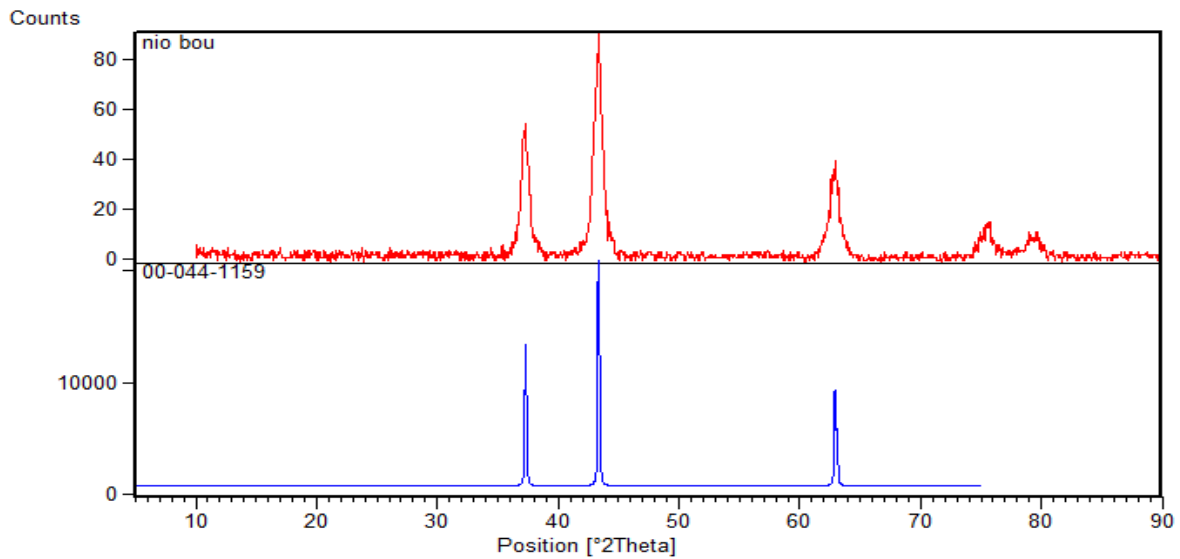


Figure III .10. XRD patterns of NiO with file ASTM (N°00-044-1159).

### III.3.3. Particles Size Distribution Analysis

The particle size is used to determine the size of the elementary particles which constitute the sets of grains of various substances and the statistical frequency of the different grain sizes in the set studied these measurements were carried out by a particle size of the type: **Malvern Mastersizer 2000/3000** the size distribution of the grains in a size range between 0.02  $\mu\text{m}$  and 2000  $\mu\text{m}$  the following figures show the grain size distribution of the oxides.

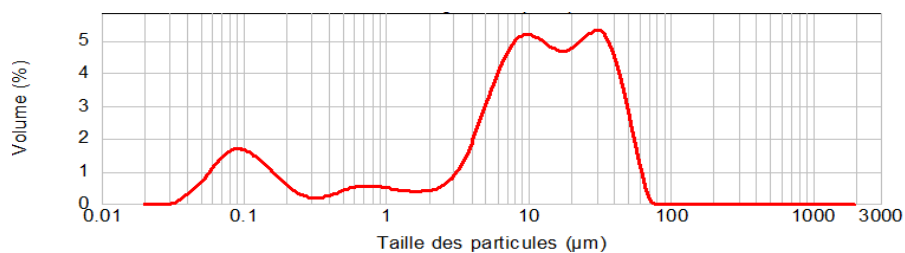
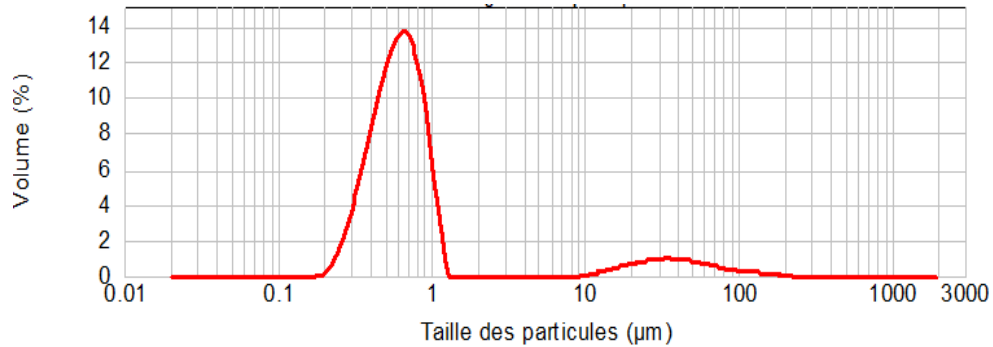


Figure III .11. The particle size distribution of  $\text{TiO}_2$  powder.

Figure shows a particle size distribution four modes in numbers of particles the first mode whose peak is centred at 0.1 $\mu\text{m}$  of the volume distribution is 1.8%, followed by a second mode of 0.75% of the distribution of which the diameter of the particles 0.75  $\mu\text{m}$  also followed by third

mode of 5.2% of the distribution of which the diameter of the particles 10  $\mu\text{m}$  and a fourth mode of 5.5% of the distribution of which the diameter of the particles 60  $\mu\text{m}$ .



**Figure III .12.** The particle size distribution of NiO powder.

The results show in the figure shows a particle size distribution a single mode of the nanoscale particles the mode whose peak is centred at 0.75  $\mu\text{m}$  of the volume distribution is 14%.

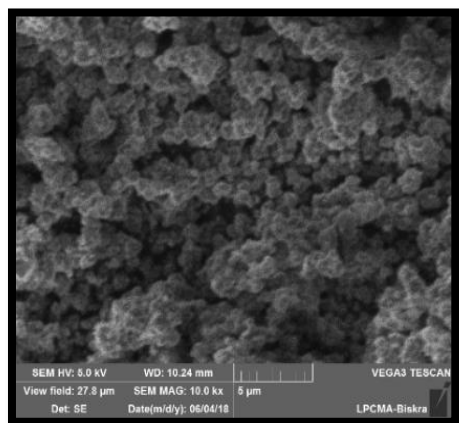
**Table III.1** Particles sizes of different oxides

Oxides	Particles sizes ( $\mu\text{m}$ )				Volume%			
	0.1	0.75	10	60	1.8	0.75	5.2	5.5
TiO <sub>2</sub>	0.1	0.75	10	60	1.8	0.75	5.2	5.5
NiO	0.75				14			

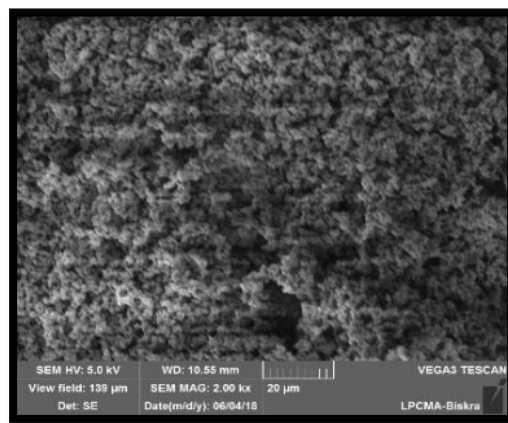
From the comparison of the previous results it is observed that the NiO powder has a nanometric population compared to that of TiO<sub>2</sub> and ZnO which have a micrometric distribution, i.e. their specific surface area is very high, so we conclude that the distribution depends on the duration grinding, dispersion.

III.3.4.SEM Analysis

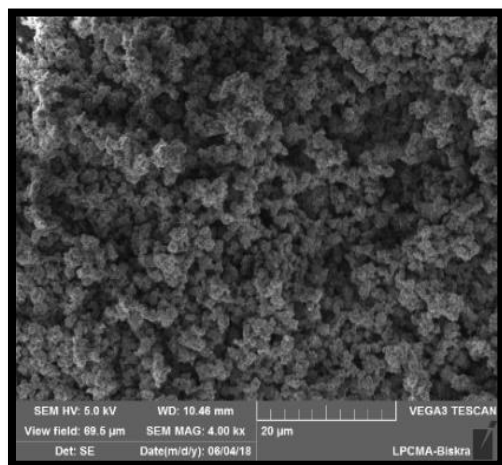
❖ SEM TiO<sub>2</sub>



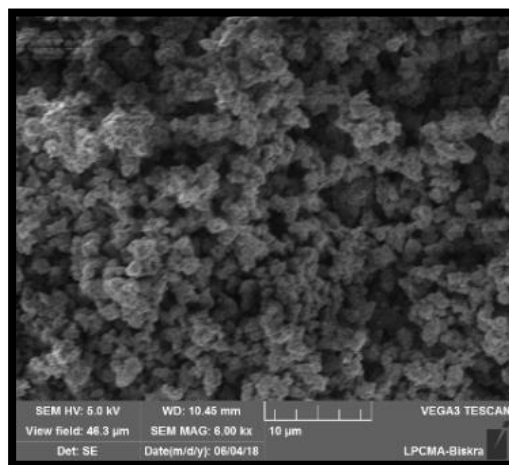
**-A-**



**-B-**



**-C-**



**-D-**

Figure III.13. SEM images of TiO<sub>2</sub> powder.

**A= grossesX1000**

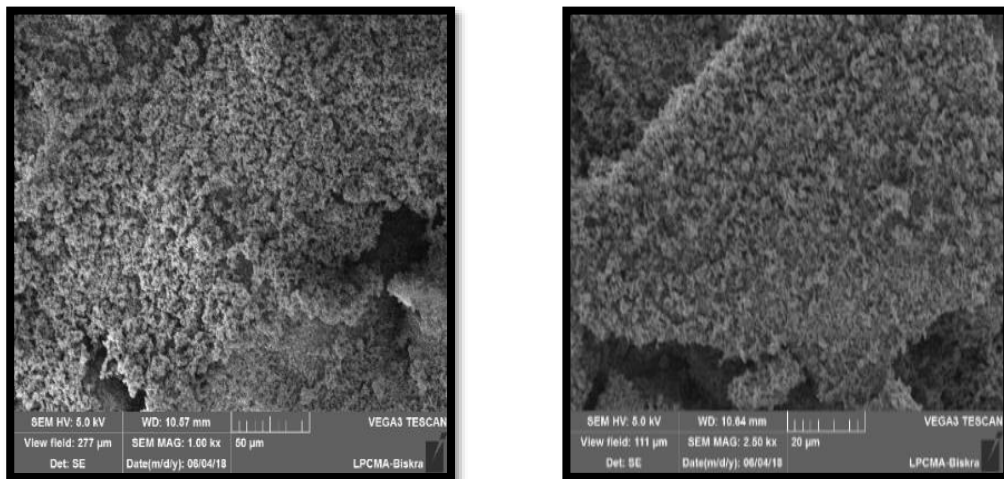
**B= grossesX2000**

**C= grosses X4000**

**D= grossesX6000**

The morphology of the artificial  $\text{TiO}_2$  powder has been investigated using Field Emission Scanning Electron Microscope. The FESEM images of  $\text{TiO}_2$  powder as shown in (figure III.13). The  $\text{TiO}_2$  powder have beehive shaped particles dimensions in the range between with 60-100 nm.

❖ SEM ZnO:



**-A-**

**-B**

**Figure III.14.** SEM images of ZnO powder.

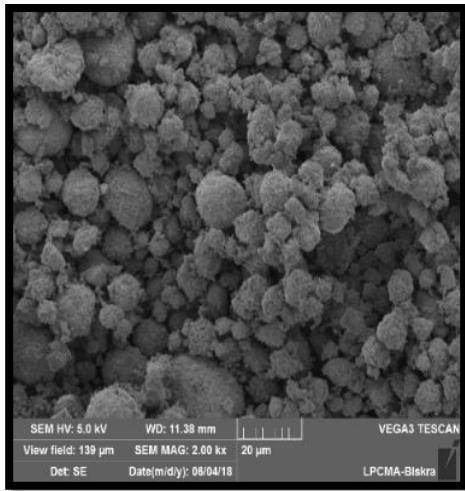
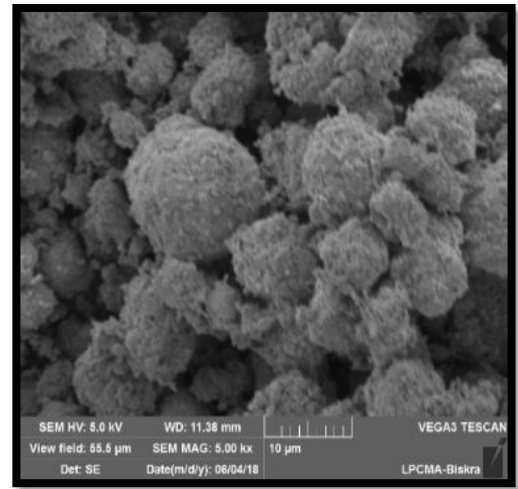
**A= grossesX1000**

**B= grossesX2000**

The SEM images of ZnO powder are given in (Figure III.14). The SEM images of ZnO powder shows undefined coarse morphology. The non-uniform particles are agglomerated and forms irregular shaped particles.



## ❖ SEM NiO

**-A-****-B-****Figure III.15.** SEM images of NiO powder**A= grossesX2000****B=grossesX5000**

The morphology of the NiO nanoparticles has been investigated using Field Emission Scanning Electron Microscope. The FESEM images of NiO nanoparticles as shown in (figure III. 15). The NiO nanoparticles have spherical shaped particles with average particle size of 64 nm.

### III.4. Photocatalytic test

The photocatalytic degradation can be achieved by artificial light and the addition of catalysts as (TiO<sub>2</sub>, ZnO, NiO), which will be studied in this chapter by verifying the factors that can influence this method.

The spectral evolution and the measurements of the absorption of the prepared solutions of the dyes (methylene blue, methyl orange, bromothymol blue were followed by spectrometry. The spectrometer used is of **Uviline9400** type and the wavelengths studied are between 200-800 nm.

To arrive at the optimal conditions, we will study the effect of different parameters on the photocatalytic activity of oxides.

To estimate the photocatalytic capacity (activity) of the oxides, three solutions of three different dyes are prepared at different concentrations. The orange methyl solution of concentration  $C = 1.5 \times 10^{-5}$  mol / L with a mass of  $m = 0.005$  g is prepared. a volume of 1000 ml and using TiO<sub>2</sub> as a photocatalyst, then methylene blue solution of concentration  $C = 1.5 \times 10^{-4}$  mol / L with a mass  $m = 0.00479$  g in a volume of 1000 ml and ZnO is used as a photocatalyst. Thirdly, the bromothymol blue solution of concentration  $C = 1.5 \times 10^{-4}$  mol / L with a mass  $m = 0.00936$  g in a volume of 1000 ml is prepared and NiO is used as a photocatalyst.

- Lamps of different light energies are used 15 w
- We change the concentrations of TiO<sub>2</sub>, ZnO, NiO: 0.5,1 and 2 mg / 1ml
- Finally, the evolution of the degradation each 15 min: 0,15,30,45,1h

The photodegradation of dyes is followed by the decrease of its absorbance either in the UV or in the visible

Firstly, the degradation of the dyes without light and without photocatalyst was tested for 24 h, a stability was found in the absorbances of the dyes, which confirms that the oxides act as a photocatalyst

The following table presents the initial evolution of photocatalytic degradation of dyes with and without light for 24 hours:

**Table III.2** Initial photodegradation tests of MO, MB, BB.

Colorants	Orange methyl( $\lambda=465\text{nm}$ )	Methylene blue( $\lambda=664\text{nm}$ )	Bromothymol blue( $\lambda=432\text{nm}$ )
t=0	$A_{\text{max}} = 2.023$	$A_{\text{max}} = 0.448$	$A_{\text{max}} = 0.086$
t=24h without light	$A_{\text{max}} = 2.020$	$A_{\text{max}} = 0.434$	$A_{\text{max}} = 0.083$
t=24h with light	$A_{\text{max}} = 2.017$	$A_{\text{max}} = 0.403$	$A_{\text{max}} = 0.069$

The results obtained show that the OM, MB, BB have been degraded with light and thus a decrease in absorbance, for these cases the degradation without light has been almost negligible and the decrease of the absorbance  $A_{\text{max}}$  is very low for this. attempts have been made to introduce different oxides such as  $\text{TiO}_2$ ,  $\text{ZnO}$ ,  $\text{NiO}$  photocatalyst and then study the factors influencing the photocatalytic reaction: the concentration of the oxides, the time to have an observable decrease in absorbance and a better photodegradation result.

#### **III.4.1. Effects of oxides concentration ( $\text{TiO}_2$ , $\text{ZnO}$ , $\text{NiO}$ ) and time**

For the study of the influence of the concentration and the time on the photodegradation, the concentration of the oxides  $\text{TiO}_2$ ,  $\text{ZnO}$ ,  $\text{NiO}$  (0.5,1,2mg / 1ml) will be changed each time, with a duration of treatment between 15min and 1 hour with a lamp of 15 w.

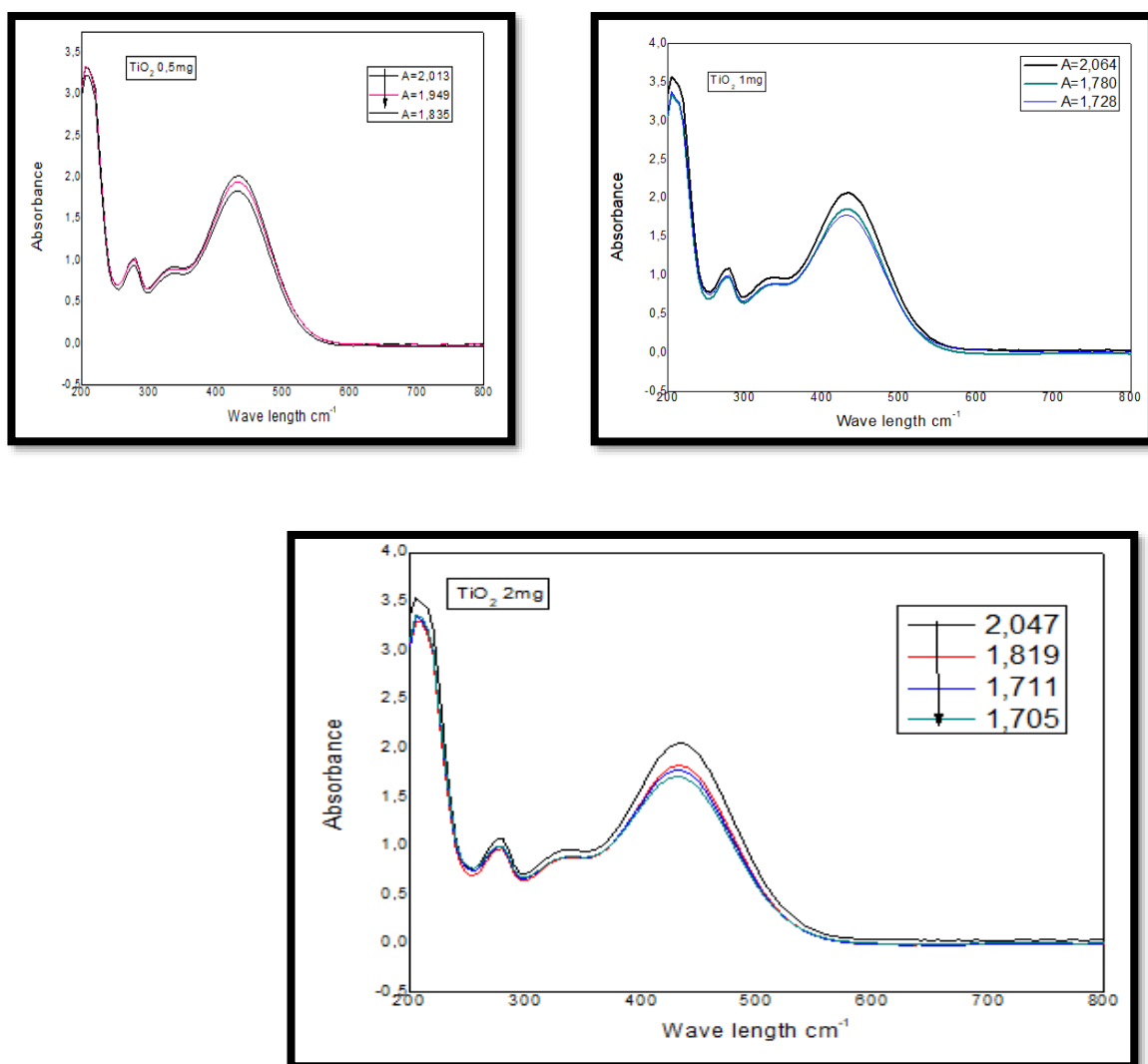


**Figure III.16.** The visible UV spectrums of OM photodegraded under the effects of TiO<sub>2</sub> concentration with time.

It is noted that the decrease in the absorbance of the OM is accompanied by the increase in the concentration of oxide TiO<sub>2</sub>, so a good degradation of the OM depends on the increase in the concentration of the TiO<sub>2</sub> catalyst and the increase of the time of reaction. The following table presents the measurements of the absorbance with change of concentration in oxide TiO<sub>2</sub> and time.

**Table III.3** The evolution of absorbance by function of concentration of TiO<sub>2</sub> and time.

t=0	A <sub>max</sub> = 2.013	λ <sub>max</sub> = 465nm
C : 0.5mg/1ml	A <sub>max</sub> = 1.949	λ <sub>max</sub> = 465nm
C : 1mg/1ml	A <sub>max</sub> = 1.835	λ <sub>max</sub> = 465nm
C : 2mg/1ml	A <sub>max</sub> =1.809	λ <sub>max</sub> = 465nm

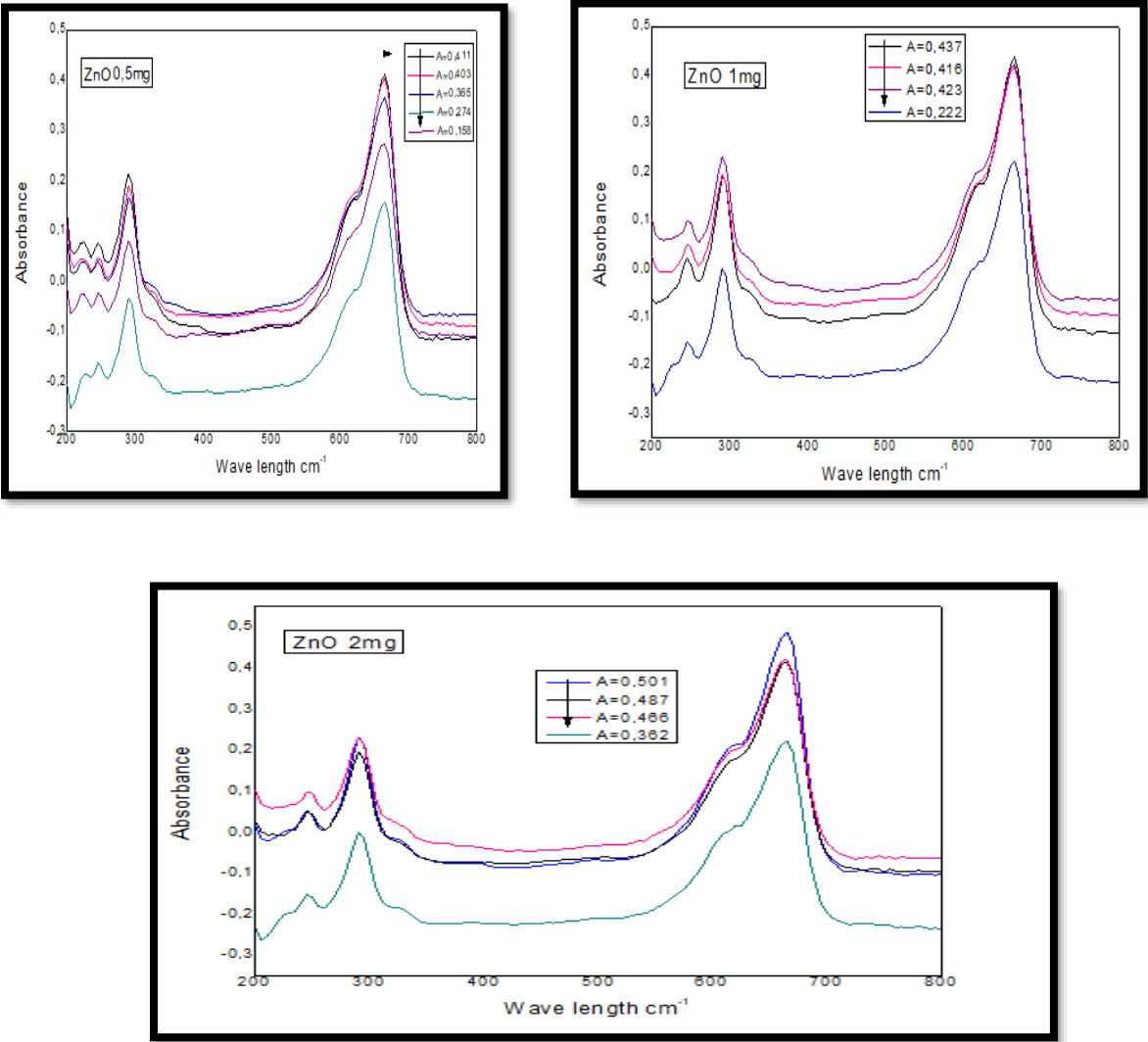


**Figure III.17.** The visible UV spectrums of MB photodegraded under the effects of ZnO concentration with time.

It is noted that the decrease in the absorbance of the MB is accompanied by the increase in the concentration of oxide ZnO, so a good degradation of the MB depends on the increase in the concentration of the ZnO catalyst.

The following table presents the measurements of the absorbance with change of concentration in oxide ZnO.

**Table III.4** The evolution of absorbance by function of concentration of ZnO and time.

t=0	$A_{\max} = 0.411$	$\lambda_{\max} = 664\text{nm}$
C : 0.5mg/1ml	$A_{\max} = 0.403$	$\lambda_{\max} = 664\text{nm}$
C : 1mg/1ml	$A_{\max} = 0.274$	$\lambda_{\max} = 664\text{nm}$
C : 2mg/1ml	$A_{\max} = 0.158$	$\lambda_{\max} = 664\text{nm}$

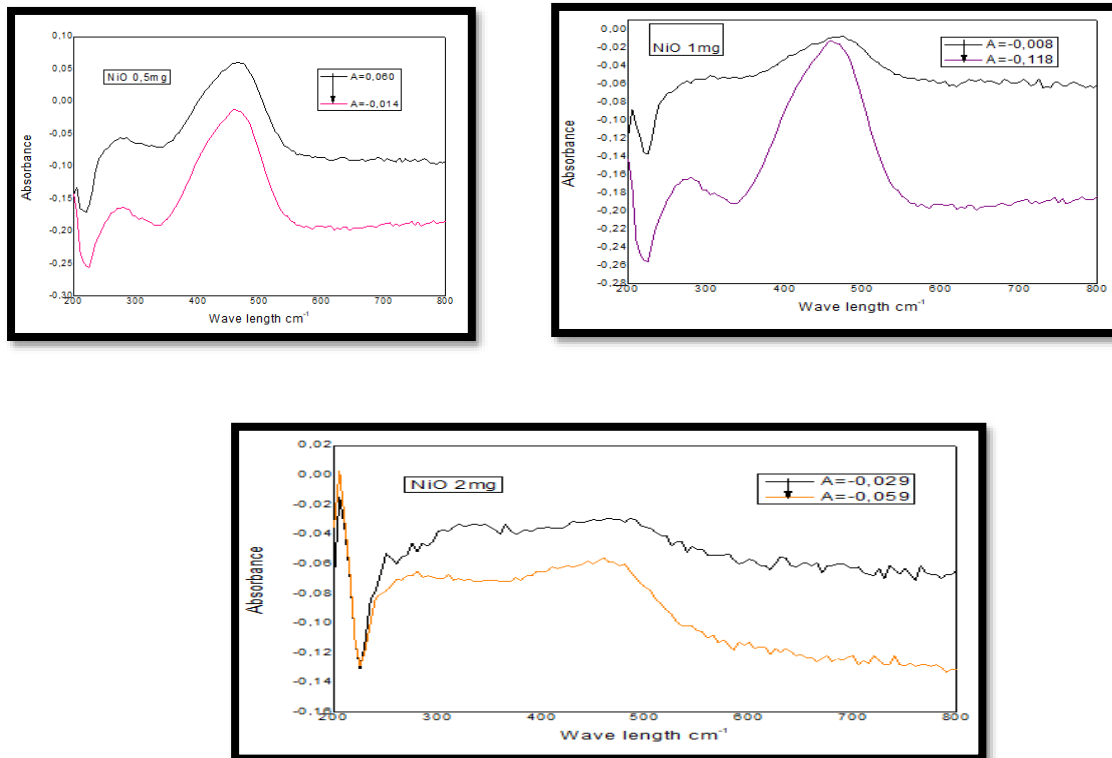


**Figure III.18.** The visible UV spectrums of BB photodegraded under the effects of NiO concentration with time.

It is noted that the decrease in the absorbance of the BB is accompanied by the increase in the concentration of oxide NiO, so a good degradation of the BB depends on the increase in the concentration of the NiO catalyst and the time of the process.

The following table presents the measurements of the absorbance with change of concentration in oxide NiO.

**Table III.5** The evolution of absorbance by function of concentration of NiO and time.

t=0	$A_{\max}=0.060$	$\lambda_{\max} = 432\text{nm}$
C= 0.5mg/1ml	$A_{\max}= - 0.014$	$\lambda_{\max} = 432\text{nm}$

## General conclusion

Photocatalytic degradation of organic pollutants is promising technology due to its advantage of degradation on pollutants instead of their transformation under ambient conditions. The process is capable of removing a wide range of organic pollutants such as pesticides, herbicides, and micro pollutants such as endocrine disrupting compounds. Although significant amount of research has been conducted on TiO<sub>2</sub> photocatalysis at laboratory scale, its application on industrial scale requires certain limitations to be addressed. However, the application of this treatment is constrained by several factors such as wide band gap (3.2eV) lack and inability of efficient and cost-effective catalyst for high photon-efficiency to utilize wider solar spectra. The effect of variables is required to be further studied in real water matrix to achieve representative results. The results achieved can be used to optimize the process and design appropriate reactor for potential large scale applications. The use of solar radiation has to be improved by virtue of the design of the photoreactor in order to reduce the cost of treatment. Further research to investigate the degradation of the real water constituents, is required to better comprehend the process applications.

A detailed study of the effect of the photocatalyst on the performance of the degradation of colorants I is achieved. The main results obtained from photocatalysis using TiO<sub>2</sub>, ZnO, NiO oxides can be summarized:

- The increase of the oxides concentrations lead to a decrease in the absorbance of the colorants in UV and Visible.
- The increase of the time of reaction leads to a decrease in the absorption, due to the increase of the charge recombination.
- The X-ray diffraction allows us to determine the crystal parameters of samples by using X' Pert High Score software, where our samples have crystal structures as follows:

TiO<sub>2</sub>:

Anatase Syn:

Crystal system hexagonal with space group P63mc and parameters  
 $a=3.2498$ ,  $b=3.2498$ ,  $c=5.2066$ , ( $\alpha=\beta\neq\gamma$ )



ZnO: Crystal system tetragonal with space group 141/amd and parameters  $a=3.7852$ ,  $b=3.7852$ ,  $c=9.5139$ , ( $\alpha=\beta=\gamma$ ).

NiO: Crystal system rhombohedral with space group R-3m and parameters  $a=2.9552$ ,  $b=2.9552$ ,  $c=7.2275$ , ( $\alpha=\beta\neq\gamma$ ).

- The Infrared allowed to determine the different bond existed for our samples:  
Vibration patterns for (Ti-O) at  $886\text{ cm}^{-1}$ , (Zn-O) at  $596\text{ cm}^{-1}$ , (Ni-O) at  $460\text{ cm}^{-1}$ .
- The Particles size distribution presented different modes where we can say about NiO is a nanoparticle diameter less than  $1\mu\text{m}$ .
- SEM analysis confirmed that there are different shapes as spherical for NiO, beehive for  $\text{TiO}_2$  and agglomeration for ZnO.
- For photocatalytic tests we conclude that the photodegradation of OM, MB, BB increases with increasing of the photocatalyst concentration and the time.
- As a perspective, the rest of this work is to study the effect of other parameters: light energy, lamps used, crystallinity, pH, temperature, and why not solar energy as a source of natural light energy.

## Abstract

Traditional chemical, physical and biological processes for treating wastewater containing textile dyes have such disadvantages as high cost, high energy requirement and generation of secondary pollution during treatment process. The advanced oxidation processes (AOPs) technology has been attracting growing attention for the decomposition of organic dyes. Such processes are based on the light-enhanced generation of highly reactive hydroxyl radicals, which oxidize the organic matter in solution and convert it completely into water, CO<sub>2</sub> and inorganic compounds. In this presentation, the photocatalytic degradation of dyes in aqueous solution using TiO<sub>2</sub>, ZnO, NiO as photocatalyst under solar and UV irradiation has been reviewed. It is observed that the degradation of dyes depends on several parameters such as pH, catalyst concentration, substrate concentration and the presence of oxidants. Reaction temperature and the intensity of light also affect the degradation of dyes. Particle size, BET surface area and different mineral forms of TiO<sub>2</sub>, ZnO, NiO also have influence on the degradation rate.

## Résumé

Les procédés chimiques, physiques et biologiques traditionnels pour le traitement des eaux usées contenant des colorants textiles présentent des inconvénients tels qu'un coût élevé, des besoins énergétiques élevés et la génération d'une pollution secondaire pendant le processus de traitement. La technologie des procédés d'oxydation avancée (AOP)s a attiré de plus en plus l'attention sur la décomposition des colorants organiques. Ces processus sont basés sur la génération de radicaux hydroxyles hautement réactifs, qui oxydent la matière organique en solution et la transforment complètement en eau, en CO<sub>2</sub> et en composés inorganiques. Dans cette présentation, la dégradation photocatalytique des colorants en solution aqueuse à l'aide de TiO<sub>2</sub>, ZnO, NiO comme photocatalyseur sous irradiation solaire et UV a été revue. On observe que la dégradation des colorants dépend de plusieurs paramètres tels que le pH, la concentration du catalyseur, la concentration du substrat et la présence d'oxydants. La température de réaction et l'intensité de la lumière affectent également la dégradation des colorants. La taille des particules, la surface BET et différentes formes minérales de TiO<sub>2</sub>, ZnO, NiO ont également une influence sur la vitesse de dégradation.

## ملخص

إن العمليات الكيميائية والفيزيائية والبيولوجية التقليدية لمعالجة مياه الصرف المحتوية على الأصباغ النسيجية لها عيوب مثل التكلفة المرتفعة واحتياجات الطاقة العالية وتوليد التلوث الثانوي أثناء عملية المعالجة. وقد اجتذبت تقنية عمليات الأكسدة المتقدمة (AOPs) اهتمامًا متزايدًا بتحلل الأصباغ العضوية. وتستند مثل هذه العمليات إلى الجيل المعزز بالضوء من جذور الهيدروكسيل شديدة التفاعل، التي تؤدي إلى أكسدة المادة العضوية في المحلول وتحويلها بالكامل إلى ماء، وثاني أكسيد الكربون، ومركبات غير عضوية. في هذه المذكرة، تمت مراجعة التحلل الضوئي للأصباغ في محلول مائي باستخدام TiO<sub>2</sub>، NiO، ZnO كمحفز ضوئي تحت إشعاع الضوء والأشعة فوق البنفسجية. ويلاحظ أن تدهور الصبغات يعتمد على عدة عوامل مثل الرقم الهيدروجيني وتركيز المحفز وتركيز الركيزة ووجود المؤكسدات. درجة حرارة التفاعل وشدة الضوء تؤثر أيضًا على تدهور الأصباغ. حجم الجسيمات، مساحة سطح BET لها أيضًا تأثير على معدل التحلل وأشكال معدنية مختلفة مثل ZnO، NiO، TiO<sub>2</sub>.

## References

- [1] Fox M., Photocatalytic Oxidation of Organic Substances. In: Kluwer (ed.) Photocatalysis and Environment: Trends and Applications. New York Academic Publishers: 1988. p. 445–467.
- [2] H.D. Roth, *Angew. Chem.* 28 (1989) 1193–1207
- [3] J.E. Pacheco, M. Prairie, L. Evans, L. Yellowhorse, Proceedings 25th Intersociety Energy Conversion Engineering Conference, Reno, Nevada, 1990, pp. 141–145.
- [4] S.E. Braslavsky, A.M. Braun, A.E. Cassano, A.V. Emeline, M.I. Litter, L. Palmisano, V.N. Parmon, N. Serpone, *Pure Appl. Chem.* 83 (2011) 931–1014.
- [5] M. Mrowetz, W. Balcerski, A.J. Colussi, M.R. Hoffmann, *J. Phys. Chem. B* 108 (2004) 17269–17273..
- [6] M. Ni, M.K.H. Leung, D.Y.C. Leung, K. Sumathy, *Renew. Sustain. Energy Rev.* 11 (2007) 401–425.
- [7] R. Vinu, D.G. Madras, *J. Indian Inst. Sci.* 90 (2010) 189–230.
- [8] A. Fujishima, K. Hashimoto, T. Watanabe, *TiO<sub>2</sub> Photocatalysis: Fundamentals and Applications*, BKC Inc., Tokyo, 1999
- [9] Wang, Y. Lu, W. Hwang, W. Chen, *Journal of the European Ceramic Society*, 30 (2010) 503. Yang, H
- [10] J. Emsley, *Titanium. Nature's Building Blocks: An A–Z Guide to the Elements*, Oxford University Press, Oxford, England, 2001.
- [11] A. Sadao, *II–VI Compound Semiconductors*, Kluwer Academic Publishers, Massachusetts, USA, 2004.
- [12] Z.L. Wang, Nanostructures of zinc oxide, *Mater. Today* 7 (6) (2004) 26–33.
- [13] E. Formo, E. Lee, D. Campbell, Y. Xia, Functionalization of electrospun TiO<sub>2</sub> nanofibers

with Pt nanoparticles and nanowires for catalytic applications, *Nanoletters* 8 (2) (2008)

668–672.

[14] U.G. Akpan, B.H. Hameed School of Chemical Engineering, Engineering Campus, Universiti Sains Malaysia, 14300 Nibong Tebal, Penang, Malaysia.

[15] <http://leaudansmonlabo.net/information/technologies-purification-eau/>.

[16] these *presentee en vue de l'obtention du diplome de doctorat en Etude comparative de la dégradation photochimique et photocatalytique de quatre colorants: Impact de la structure chimique et corrélation entre l'adsorption et l'activité photocatalytique de TiO<sub>2</sub> Spécialité Chimie physique et analytique* Par Nour BOUANIMBA Soutenu le 12 juin 2014

[17] Marcel, Lecomte. “neufchateau bleu de methylene” .Cercle des Mycologues.Luxembourg 10,B-6840.

[18] <http://www.academicjournals.org/IJPS>

[19] Hach company, bromothymol bleu, 1990, (msds information handling services), 9911-630 f 03..

[20] Recent developments in photocatalytic water treatment technology: A review Meng Nan Chong a,b, Bo Jin a,b,c,\* , Christopher W.K. Chow c, Chris Saint c a School of Chemical Engineering, The University of Adelaide, 5005 Adelaide, Australia

[21] Cezoir, David-Alexandre. *Traitement d'eaux huileuses par photocatalyses hétérogène application à la depollution des eaux de cales*. Diss .Université Claude Bernard\_Lyon I, 2011.

[22] Step synthesis and photocatalytic activity of NiO/graphene nanocomposite under UV and visible light as an effective photocatalyst Faezeh Soofivand, Masoud Salavati-Niasari\* Institute of Nano Science and Nano Technology, University of Kashan, Kashan, P. O. Box. 87317-51167, Islamic Republic of Iran.

[23] *Modern Chemical Techniques*, RSC, 1992. The Education Department, The Royal Society of Chemistry, Burlington house, Piccadilly, London W1J 0BA.



## Abbreviations

μm	Micrometer
CB	Conduction band
VB	Valence band
CO <sub>2</sub>	Carbon dioxide
E <sub>g</sub>	Band gap
eV	Electron volt
TiO <sub>2</sub>	Titanium dioxide
ZnO	Zinc oxide
NiO	Nickel oxide
OM	Orange Methyl
MB	Methylene blue
BB	Bromothymol blue
XDR	X-Ray diffraction
FE-SEM	Field emission scanning electron microscopy
UV	Ultraviolet
FT-IR	Fourier transform infrared
AOP	Advanced Oxidation Process
PSD	Particle Size Distribution
BET	Brunauer-Emmett-Teller Theory of Specific Surface Area

## Annexe

✚ The file ASTM N°00-021-1272 of TiO<sub>2</sub> presented on the following figure:

### Name and formula

Reference code:	00-021-1272
Mineral name:	Anatase, syn
PDF index name:	Titanium Oxide
Empirical formula:	O <sub>2</sub> Ti
Chemical formula:	TiO <sub>2</sub>

### Crystallographic parameters

Crystal system:	Tetragonal
Space group:	I41/amd
Space group number:	141
a (Å):	3,7852
b (Å):	3,7852
c (Å):	9,5139
Alpha (°):	90,0000

Beta (°): 90,0000

Gamma (°): 90,0000

Calculated density (g/cm<sup>3</sup>): 3,89

Volume of cell (10<sup>6</sup> pm<sup>3</sup>): 136,31

Z: 4,00

RIR: 3,30

### **Subfiles and Quality**

Subfiles: Inorganic  
Mineral  
Alloy, metal or intermetallic  
Corrosion  
Common Phase  
Educational pattern  
Forensic  
NBS pattern  
Pharmaceutical  
Pigment/Dye

Quality: Star (S)

### **Comments**



Color: Colorless

General comments: Anatase and another polymorph, brookite (orthorhombic), are converted to rutile (tetragonal) by heating above 700 C.

Pattern reviewed by Holzer, J., McCarthy, G., North Dakota State Univ, Fargo, North Dakota, USA, *ICDD Grant-in-Aid* (1990). Agrees well with experimental and calculated patterns.

Sample source: Sample obtained from National Lead Co., South Amboy, New Jersey, USA.

Additional pattern: See ICSD 9852 (PDF 01-071-1166).

Validated by calculated pattern.

Temperature: Pattern taken at 25 C.

### **References**

Primary reference: *Natl. Bur. Stand. (U.S.) Monogr. 25, 7, 82, (1969)*

### **Peak list**

<u>No.</u>	<u>h</u>	<u>k</u>	<u>l</u>	<u>d [Å]</u>	<u>2Theta[deg]</u>	<u>I [%]</u>
1	1	0	1	3,52000	25,281	100,0
2	1	0	3	2,43100	36,947	10,0
3	0	0	4	2,37800	37,801	20,0
4	1	1	2	2,33200	38,576	10,0
5	2	0	0	1,89200	48,050	35,0
6	1	0	5	1,69990	53,891	20,0
7	2	1	1	1,66650	55,062	20,0

8	2	1	3	1,49300	62,121	4,0
9	2	0	4	1,48080	62,690	14,0
10	1	1	6	1,36410	68,762	6,0
11	2	2	0	1,33780	70,311	6,0
12	1	0	7	1,27950	74,031	2,0
13	2	1	5	1,26490	75,032	10,0
14	3	0	1	1,25090	76,020	4,0
15	0	0	8	1,18940	80,727	2,0
16	3	0	3	1,17250	82,139	2,0
17	2	2	4	1,16640	82,662	6,0
18	3	1	2	1,16080	83,149	4,0
19	2	1	7	1,06000	93,221	2,0
20	3	0	5	1,05170	94,182	4,0
21	3	2	1	1,04360	95,143	4,0
22	1	0	9	1,01820	98,319	2,0
23	2	0	8	1,00700	99,804	2,0
24	3	2	3	0,99670	101,221	2,0
25	3	1	6	0,95550	107,448	4,0
26	4	0	0	0,94640	108,963	4,0
27	3	0	7	0,92460	112,841	2,0
28	3	2	5	0,91920	113,861	2,0
29	4	1	1	0,91380	114,909	2,0
30	2	1	9	0,89660	118,439	4,0
31	2	2	8	0,88900	120,104	2,0
32	4	1	3	0,88190	121,725	2,0

33	4	0	4	0,87930	122,336	2,0
34	4	2	0	0,84640	131,036	2,0
35	3	2	7	0,83080	135,998	2,0
36	4	1	5	0,82680	137,391	4,0
37	3	0	9	0,81020	143,888	2,0
38	4	2	4	0,79740	150,039	4,0
39	0	0	12	0,79280	152,634	2,0

### **Stick Pattern**

File ASTM N°00-044-1159 of Zinc oxide

✚ The file ASTM N°00-036-1451 of ZnO presented on the following figure:

### **Name and formula**

Reference code: 00-036-1451

Mineral name: Zincite, syn

Common name: Chinese white

PDF index name: Zinc Oxide

Empirical formula: OZn

Chemical formula: ZnO

## **Crystallographic parameters**

Crystal system: Hexagonal

Space group: P63mc

Space group number: 186

a (Å): 3,2498

b (Å): 3,2498

c (Å): 5,2066

Alpha (°): 90,0000

Beta (°): 90,0000

Gamma (°): 120,0000

Volume of cell ( $10^6 \text{ pm}^3$ ): 47,62

Z: 2,00

RIR: -

## **Subfiles and Quality**

Subfiles: Inorganic

Mineral

Alloy, metal or intermetallic

Corrosion  
Common Phase  
Educational pattern  
Forensic  
NBS pattern  
Pharmaceutical  
Pigment/Dye

Quality: Star (S)

### **Comments**

Color: Colorless

General comments: The structure was determined by Bragg (1) and refined by Abrahams, Bernstein (2).

Sample source: The sample was obtained from the New Jersey Zinc Co., Bethlehem, Pennsylvania, USA.

Optical data: B=2.013, Q=2.029, Sign=+

Polymorphism: A high pressure cubic NaCl-type of ZnO is reported by Bates et al. (3) and a cubic, sphalerite type is reported by Radczewski, Schicht (4).

Additional pattern: To replace 00-005-0664 (5).

See ICSD 31052 (PDF 01-075-1526).

Temperature: The approximate temperature of data collection was 26 C.

Powder data (additional reference): References to other early patterns may be found in reference (5).

### **References**

Primary reference: McMurdie, H., Morris, M., Evans, E., Paretzkin, B., Wong-Ng, W., Ettlinger, L., Hubbard, C., *Powder Diffraction*, **1**, 76, (1986)

Structure : 1. Bragg, W., *Philos. Mag.*, **39**, 647, (1920)

Optical data: *Dana's System of Mineralogy, 7th Ed.*, **I**, 504

Polymorphism: 3. Bates, C., White, W., Roy, R., *Science*, **137**, 993, (1962)

Additional pattern: 5. Swanson, H., Fuyat, R., *Natl. Bur. Stand. (U.S.), Circ. 539*, **2**, 25, (1953)

### **Peak list**

No.	h	k	l	d [Å]	2Theta[deg]	I [%]
1	1	0	0	2,81430	31,770	57,0
2	0	0	2	2,60332	34,422	44,0
3	1	0	1	2,47592	36,253	100,0
4	1	0	2	1,91114	47,539	23,0
5	1	1	0	1,62472	56,603	32,0
6	1	0	3	1,47712	62,864	29,0
7	2	0	0	1,40715	66,380	4,0
8	1	1	2	1,37818	67,963	23,0
9	2	0	1	1,35825	69,100	11,0
10	0	0	4	1,30174	72,562	2,0
11	2	0	2	1,23801	76,955	4,0
12	1	0	4	1,18162	81,370	1,0
13	2	0	3	1,09312	89,607	7,0
14	2	1	0	1,06384	92,784	3,0
15	2	1	1	1,04226	95,304	6,0

16	1	1	4	1,01595	98,613	4,0
17	2	1	2	0,98464	102,946	2,0
18	1	0	5	0,97663	104,134	5,0
19	2	0	4	0,95561	107,430	1,0
20	3	0	0	0,93812	110,392	3,0
21	2	1	3	0,90694	116,279	8,0
22	3	0	2	0,88256	121,572	4,0
23	0	0	6	0,86768	125,188	1,0
24	2	0	5	0,83703	133,932	3,0
25	1	0	6	0,82928	136,521	1,0
26	2	1	4	0,82370	138,513	2,0
27	2	2	0	0,81247	142,918	3,0

### **Stick Pattern**

File ASTM N°00-036-1451 of Zinc oxide

 The file ASTM N°00-044-1159 of NiO presented on the following figure:

### **Name and formula**

Reference code: 00-044-1159

PDF index name: Nickel Oxide

Empirical formula: NiO

Chemical formula: NiO

## **Crystallographic parameters**

Crystal system: Rhombohedral

Space group: R-3m

Space group number: 166

a (Å): 2,9552

b (Å): 2,9552

c (Å): 7,2275

Alpha (°): 90,0000

Beta (°): 90,0000

Gamma (°): 120,0000

Calculated density (g/cm<sup>3</sup>): 6,81

Volume of cell (10<sup>6</sup> pm<sup>3</sup>): 54,66

Z: 3,00

RIR: 2,10

## **Subfiles and Quality**

Subfiles: Inorganic



Alloy, metal or intermetallic  
Corrosion  
Forensic  
Quality: Star (S)

### **Comments**

Colors: Light green  
Sample preparation: Sample obtained from Merck (puriss.). For better crystallization, annealed at 1300 C for 5 hours and quenched.  
Additional pattern: Second cubic polymorph known (see 00-004-0835).  
To replace 00-022-1189.  
Temperature: Pattern taken at 22 C.

### **References**

Primary reference: Wies, S., Eysel W., Mineral. -Petrograph., Institut der Universitaet Heidelberg, Germany., *ICDD Grant-in-Aid*, (1992)

### **Peak list**

No.	h	k	l	d [Å]	2Theta[deg]	I [%]
1	1	0	1	2,41197	37,249	60,0
2	0	1	2	2,08849	43,287	100,0
3	1	1	0	1,47733	62,854	30,0
4	1	0	4	1,47607	62,914	25,0
5	1	1	3	1,25955	75,406	14,0
6	2	0	2	1,20624	79,374	9,0
7	0	0	6	1,20460	79,504	4,0

8	0	2	4	1,04433	95,055	6,0
9	2	1	1	0,95882	106,909	4,0
10	2	0	5	0,95817	107,013	2,0
11	1	0	7	0,95761	107,104	2,0
12	1	2	2	0,93437	111,057	7,0
13	1	1	6	0,93363	111,188	7,0
14	2	1	4	0,85282	129,174	7,0
15	0	1	8	0,85187	129,443	3,0

### **Stick Pattern**

File ASTM N°00-044-1159 of Nickel oxide